VGLL2 and TEAD1 fusion proteins drive YAP/TAZ-independent tumorigenesis by engaging p300

Susu Guo[1,#], Xiaodi Hu[2,#], Jennifer L. Cotton[2], Lifang Ma[1], Qi Li[2, 3], Jiangtao Cui[1], Yongjie Wang[1], Ritesh P. Thakare[2], Zhipeng Tao[4], Y. Tony Ip[3], Xu Wu[4], Jiayi Wang[1,*], Junhao Mao[2,*]

[1] Department of Clinical Laboratory, Shanghai Chest Hospital, Shanghai Jiao Tong University School of Medicine, No 241, West Huaihai Road, Shanghai, P. R., 200030, China.
[2] Department of Molecular, Cell and Cancer Biology, University of Massachusetts Chan Medical School, Worcester, Massachusetts, 01605, USA.
[3] Program in Molecular Medicine, University of Massachusetts Chan Medical School, Worcester, Massachusetts, 01605, USA.
[4] Cutaneous Biology Research Center, Massachusetts General Hospital, Harvard Medical School, Charlestown, Massachusetts, 01605, USA.

[#] Susu Guo and Xiaodi Hu contributed equally to this work.

***Corresponding author**
Junhao Mao, Department of Molecular, Cell and Cancer Biology, University of Massachusetts Chan Medical School, Worcester, Massachusetts, 01605, USA
Email: junhao.mao@umassmed.edu

Jiayi Wang, Department of Clinical Laboratory, Shanghai Chest Hospital, Shanghai Jiao Tong University School of Medicine, No 241, West Huaihai Road, Shanghai, P. R., 200030, China
Email: jiayi.wang@sjtu.edu.cn

Running title：VGLL2 fusion proteins induce TEAD-mediated transcription via p300

Abstract

Studies on Hippo pathway regulation of tumorigenesis largely center on YAP and TAZ, the transcriptional co-regulators of TEAD. Here, we present an oncogenic mechanism involving VGLL and TEAD fusions that is Hippo pathway-related but YAP/TAZ-independent. We characterize two recurrent fusions, VGLL2-NCOA2 and TEAD1-NCOA2, recently identified in spindle cell rhabdomyosarcoma. We demonstrate that in contrast to VGLL2 and TEAD1, the fusion proteins are strong activators of TEAD-dependent transcription, and their function does not require YAP/TAZ. Furthermore, we identify that VGLL2 and TEAD1 fusions engage specific epigenetic regulation by recruiting histone acetyltransferase p300 to control TEAD-mediated transcriptional and epigenetic landscapes. We showed that small molecule p300 inhibition can suppress fusion proteins-induced oncogenic transformation both *in vitro* and *in vivo*. Overall, our study reveals a molecular basis for VGLL involvement in cancer and provides a framework for targeting tumors carrying VGLL, TEAD, or NCOA translocations.

Keywords：VGLL2, TEAD1, NCOA2, fusion, Hippo signaling pathway, p300

Introduction

Hippo signaling, originally identified in Drosophila as an organ size control pathway, has emerged as a critical developmental pathway whose dysregulation contributes to the development and progression of a variety of human diseases, including cancer (Zheng and Pan 2019; Ma et al., 2019; Calses et al., 2019; Kulkarni et al., 2020; Piccolo et al., 2023). In the mammalian Hippo pathway, activation of the core kinase cascade, which comprises the macrophage stimulating 1/2 (MST1/2) and large tumor suppressor kinase 1/2 (LATS1/2) kinases, leads to phosphorylation, cytosolic retention, and degradation of the key transcriptional coactivators, YAP and TAZ. Upon Hippo pathway inactivation, YAP and TAZ translocate into the nucleus and interact with the TEAD family of transcription factors, thereby inducing downstream gene transcription (Zheng and Pan 2019; Ma et al., 2019; Totaro et al., 2018). Although the Hippo pathway has been implicated in human cancers, mutations or deletions of the pathway components, such as the MST1/2 or LATS1/2 kinases, are rarely detected in cancers. The focus on Hippo involvement in tumorigenesis has been on the transcriptional co-activators, YAP and TAZ, whose up-regulation or nuclear accumulation has been reported in various cancer types (Piccolo et al., 2023; Thompson 2020; Franklin et al., 2023). In addition, recent studies identified YAP and TAZ fusion proteins as oncogenic drivers in several tumors, including epithelioid hemangioendothelioma, supratentorial ependymoma, porocarcinoma, epithelioid fibrosarcoma, and NF2-wild type meningioma (Driskill et al., 2021; Seavey et al., 2021; Merritt et al., 2021; Szulzewsky et al., 2021; Szulzewsky et al., 2022; Garcia et al., 2022), further highlighting the critical role of YAP/TAZ in tumorigenesis.

The mammalian VGLL family proteins (VGLL1-4) are expressed in various tissues, and it is thought that VGLL proteins carry out their cellular function via interaction with TEADs (Faucheux et al., 2010; Pobbati et al., 2012; Simon et al., 2016; Yamaguchi 2020). However, in comparison to YAP and TAZ, little is known about their functional regulation. Among the VGLL proteins, VGLL4 and its Drosophila homolog Tgi have been demonstrated as transcriptional repressors by competing with YAP/TAZ binding to TEAD through two TONDU (TDU) domains (Koontz et al., 2013; Cai et al., 2022; Zhang et al., 2014; Li et al., 2023). In contrast, the precise function of VGLL1-3 in both normal and tumor cells and how they influence Hippo/YAP signaling and affect TEAD transcriptional output remain poorly understood.

Several recent studies have identified the recurrent rearrangement of the VGLL2 and TEAD1 genes in a large subset of spindle cell rhabdomyosarcoma (scRMS), a pediatric form of RMS that is distinct from embryonic RMS (ERMS) (Alaggio et al., 2016; Tan et al., 2020; Chen et al., 2020; Cyrta et al., 2021; Whittle et al., 2022). In these fusions, VGLL2 and TEAD1 participate as 5’ partners in the recurrent translocations, and their 3’ fusion partners often involve the NCOA2 gene on 8q13.3 (Alaggio et al., 2016). Among these fusion proteins, the VGLL2-NCOA2 fusion has recently been shown to be able to drive tumor formation in zebrafish and allograft models (Watson et al., 2023). Here, we explored the molecular

mechanism underlying the oncogenic transformation of VGLL2-NCOA2 and TEAD1-NCOA2 fusion proteins. We revealed that, in comparison to VGLL2 and TEAD1, VGLL2-NCOA2 and TEAD1-NCOA2 are robust activators of TEAD-mediated transcription. We demonstrated that VGLL2-NCOA2 and TEAD1-NCOA2-controlled transcriptional activation is YAP/TAZ-independent, and these fusion proteins specifically engage the CBP/p300 epigenetic factors that are critical for their oncogenic activation.

Results

VGLL2-NCOA2 and TEAD1-NCOA2 induce TEAD-mediated transcriptional activation. In VGLL2-NCOA2 and TEAD1-NCOA2 fusions, VGLL2 and TEAD1 are 5' partners and maintain the key functional domains at the N-terminus. VGLL2 retains the TDU domain, while TEAD1 preserves its TEA DNA binding domain (Figure 1A). The 3' partners of the fusions are NCOA2, which retains its two C-terminal transcriptional activation domains (TAD) (Figure 1A). The exons and breaking points of the VGLL2, TEAD1 and NCOA2 genes involved in generating the VGLL2-NCOA2 and TEAD1-NCOA2 gene arrangement are presented in Figure 1-figure supplement 1A. To test the transcriptional activity of the fusion proteins, we utilized an 8xGIIC luciferase reporter that contains 8X TEAD DNA binding sites (TBS-Luc) (Dupont et al., 2011). When ectopically expressed in HEK293T cells, we found that, in comparison to the VGLL2, TEAD1, and NCOA2 proteins, the VGLL2-NCOA2 and TEAD1-NCOA2 fusion proteins could significantly induce the transcriptional activation of the TBS-Luc reporter, and their activity was comparable to the activated forms of YAP and TAZ, YAP^{5SA} and TAZ^{4SA}, in which the LATS kinase phosphorylation sites are mutated rendering them constitutively active (Zhao et al., 2010) (Figure 1B and C). Additionally, we showed that ectopic expression of VGLL2-NCOA2 and TEAD1-NCOA2 in HEK293T cells promotes cell proliferation (Figure 1-figure supplement 1B), mimicking the pro-growth activity of activated YAP and TAZ. Furthermore, we demonstrated that the ability of VGLL2-NCOA2 to induce downstream transcription requires both its N-terminal VGLL2 and C-terminal NCOA2 fusion parts, and this effect is dose-dependent and not affected by the 5' or 3' protein tags (Figure 1-figure supplement 1C-H).

To further characterize the downstream transcription induced by VGLL2-NCOA2 and TEAD1-NCOA2, we performed RNA-seq analysis in HEK293T cells overexpressing VGLL2-NCOA2, TEAD1-NCOA2, or YAP^{5SA} (Figure 1D and Figure 1-figure supplement 2, Supplementary File 1-3). We found that all three could robustly drive transcriptional programs in HEK293T cells, and VGLL2-NCOA2 and TEAD1-NCOA2-induced transcription clustered together and appeared to be distinct from the YAP^{5SA}-driven program (Figure 1D). However, similar to activated YAP, VGLL2-NCOA2, and TEAD1-NCOA2 fusion proteins also strongly induced the expression of *bona fide* TEAD downstream target genes, such as CTGF, CYR61, ANKRD1, and AMOTL2 (Figure 1D). This was further confirmed by RT-qPCR analysis, which showed that the transcriptional levels of CTGF, CYR61, and ANKRD1 were significantly elevated in the cells expressing VGLL2-NCOA2, TEAD1-NCOA2, or YAP^{5SA} but not in those expressing VGLL2, TEAD1, and NCOA2 (Figure 1E). Taken together, these data suggest that

unlike native VGLL2 and TEAD1, VGLL2-NCOA2 and TEAD1-NCOA2 fusion proteins function as strong activators of TEAD-mediated transcription.

VGLL2-NCOA2 and TEAD1-NCOA2-induced transcription does not require YAP and TAZ.

Next, we set out to examine how the VGLL2-NCOA2 and TEAD1-NCOA2 fusion proteins interact with YAP/TAZ and TEAD, the well-characterized transcriptional nexus in the Hippo pathway. We performed co-IP assays in HEK293T cells expressing VGLL2-NCOA2, YAP^{5SA}, and TEAD1 and demonstrated that VGLL2-NCOA2 was strongly associated with TEAD1 but not YAP^{5SA} (Figure 2A). Furthermore, we showed that VGLL2-NCOA2 could bind to the endogenous TEAD proteins; however, we did not detect a strong interaction between VGLL2-NCOA2 and endogenous YAP and TAZ proteins in HEK293T cells (Figure 2B). In addition, we compared the ability of TEAD1-NCOA2 and TEAD1 to interact with YAP and TAZ. Not surprisingly, TEAD1 was able to bind YAP/TAZ; however, the interaction between TEAD1-NCOA2 and endogenous YAP/TAZ was not detected (Figure 2C), which is consistent with the absence of the C-terminal YAP/TAZ binding domain in the TEAD1-NCOA2 fusion. Together, these co-IP assays revealed the lack of association between the VGLL2 and TEAD1 fusion proteins and YAP/TAZ, suggesting that the regulation of transcription by the fusion proteins is likely TEAD-dependent but YAP/TAZ-independent.

To examine the TEAD regulation in VGLL2-NCOA2 and TEAD1-NCOA2-mediated transcription, we first utilized a small molecule TEAD inhibitor, CP1, that was recently developed to inhibit TEAD auto-palmitoylation, leading to protein instability and transcriptional inactivation (Li et al., 2020; Sun et al., 2022). Upon treatment with the TEAD palmitoylation inhibitor CP1 in HEK293T cells transfected with YAP^{5SA}, VGLL2-NCOA2, and TEAD1-NCOA2, we found that CP1 effectively inhibited YAP^{5SA}- and VGLL2-NCOA2-induced transcriptional activation but had largely no effect on TEAD1-NCOA2-induced reporter activation (Figure 2D). The inability of CP1 to inhibit TEAD1-NCOA2 activity is likely because the TEAD1-NCOA2 fusion does not contain the auto-palmitoylation sites in the C-terminal YAP-binding domain of TEAD1. To further explore TEAD dependence, we generated a TEAD fusion dominant repressor, TEAD-ENR, which fuses its N-terminal TEA DNA-binding domain to a C-terminal Engrained repressor domain (Figure 2E and F). When co-expressed with YAP^{5SA}, VGLL2-NCOA2, and TEAD1-NCOA2 in HEK293T cells, TEAD1-ENR potently inhibited the transcriptional activation of all three proteins (Figure 2D). These results from both the TEAD inhibitor and transcriptional repressor suggest that downstream TEAD activity and TEAD DNA binding are critical for both fusion proteins.

To further examine the involvement of YAP and TAZ in VGLL2-NCOA2- and TEAD1-NCOA2-induced transcription, we used lentiviral-based shRNA to knock down the expression of YAP and TAZ in HEK293T cells (Figure 2G). We showed that VGLL2-NCOA2 could bind to endogenous TEAD proteins at similar levels in both control and YAP/TAZ-knockdown HEK293T cells (Figure 2G), suggesting its association with TEAD does not require YAP/TAZ. Furthermore, we found that both VGLL2-NCOA2 and TEAD1-NCOA2 still robustly induced the transcription of the known TEAD target genes, including CTGF,

ANKRD1, and CYR61, in HEK293T cells with YAP/TAZ knockdown (Figure 2H). Taken together, our data suggest that VGLL2-NCOA2- and TEAD1-NCOA2-induced transcriptional activation requires TEAD DNA binding but is YAP/TAZ independent.

Characterization of VGLL2-NCOA2- and YAP- controlled transcriptional and chromatin landscapes.

To understand the mechanism of how the fusion proteins may control chromatin landscapes and drive downstream transcription, we performed analyses of ATAC-seq, CUT&RUN sequencing, and RNA-seq in HEK293T cells that ectopically expressed VGLL2-NCOA2 and compared them to the epigenetic and transcriptional programs controlled by YAP^{5SA}.

By intersecting the datasets of ATAC-seq (assessing genome-wide chromatin accessibility regulated by VGLL2-NCOA2 and YAP^{5SA}), CUT&RUN (mapping both VGLL2-NCOA2 and YAP^{5SA} binding sites across the genome), and RNA-seq (transcriptome profiling in VGLL2-NCOA2 and YAP^{5SA}-expressing cells), we determined that VGLL2-NCOA2 and YAP controlled overlapping yet distinct chromatin landscapes and downstream transcriptional programs (Figure 3 and Figure 3-figure supplement 1).

In our ATAC-seq assay, the analysis of differentially accessible chromatin sites annotated to the nearest genes showed significant enrichment of Hippo pathway-related genes in both VGLL2-NCOA2 and YAP^{5SA}-expressing cells (Figure 3A-C), suggesting that VGLL2-NCOA2 and YAP^{5SA} likely drive open chromatin architecture in a shared set of genes. This is also consistent with our analysis of the genomic occupancy profiles of VGLL2-NCOA2 and YAP^{5SA} defined by CUT&RUN sequencing (Figure 3D-F and Figure 3-figure supplement 2F). Annotation of CUT&RUN peaks with respect to their nearest gene transcriptional start site (TSS) showed that both VGLL2-NCOA2 and YAP preferred to occupy distal genomic regions that are not in close proximity to the TSS (0-2kb) (Figure 3D). This is consistent with prior reports that YAP preferentially binds to distal enhancer regions (Zanconato et al., 2015; Liu et al., 2016) and indicates that the VGLL2-NCOA2 fusion protein also regulates downstream gene transcription through active enhancers.

In addition, *de novo* motif analysis of our CUT&RUN datasets revealed that the TEAD binding sequence was among the most enriched motifs in both VGLL2-NCOA2 and YAP^{5SA} CUT&RUN peaks (Figure 3E), consistent with our observation that TEAD DNA binding was essential for transcriptional activation induced by the fusion proteins (Figure 2A-F). Interestingly, the AP1 motif was also enriched in VGLL2-NCOA2 CUT&RUN peaks (Figure 3E), highlighting its proposed roles in TEAD-mediated transcription (Zanconato et al., 2015; Liu et al., 2016). Furthermore, we compared the binding profiles of the *bona fide* downstream target genes of VGLL2-NCOA2 and YAP identified in our CUT&RUN analysis, CTGF, ANKRD1, and CYR61, and showed that VGLL2-NCOA2 and YAP occupied the same genomic regions in the loci of the three genes (Figure 3F). Our analyses demonstrated that VGLL2-NCOA2 and YAP control overlapping yet distinct chromatin landscapes and occupy a shared set of genomic regions, thereby driving downstream gene transcription.

VGLL2-NCOA2 and TEAD1-NCOA2 engage p300 epigenetic regulators.

In addition to their YAP/TAZ independence, the distinct nature of transcriptional and chromatin landscapes controlled by VGLL2-NCOA2 and YAP prompted us to hypothesize that the fusion proteins might utilize different sets of epigenetic/transcriptional regulators to modify chromatin and drive gene expression. To this end, we adopted a proximity-labeling proteomics approach called BioID (Kim and Roux, 2016) to identify the potential binding partners of VGLL2-NCOA2 and TEAD1-NCOA2 and compared them to YAP and TAZ.

In our BioID proteomics screens, we tagged YAP^{5SA}, TAZ^{4SA}, VGLL2-NCOA2, and TEAD1-NCOA2 with BirA* (a promiscuous version of the biotin ligase BirA) and used them as baits to probe the proteomes associated with these proteins (Figure 4A, Supplementary File 4). By intersecting the hits associated with YAP/TAZ or VGLL2-NCOA2/TEAD1-NCOA2, we found that TEAD proteins were among the few proteins associated with all four proteins, providing validation of our BioID datasets (Figure 4A). Focusing on epigenetic and transcriptional regulators identified in the screens, we found that CBP and p300 were among the hits specifically associated with VGLL2-NCOA2 and TEAD1-NCOA2 in the BioID assays (Figure 4A).

The closely related histone acetyltransferases CBP and p300, commonly referred as CBP/p300, are known for their function to induce histone H3 lysine 27 acetylation (H3K27ac) at the promoter and enhancer regions, thereby activating gene transcription (Ogryzko et al., 1996; Bannister and Kouzarides 1996; Waddell et al., 2021; Hogg et al., 2021). More importantly, CBP/p300 has been reported to form a complex with the NCOA family proteins that play a critical role in the regulation of nuclear receptors-mediated transcription (Waddell et al., 2021; Yi et al., 2021). It is consistent with our proteomics data that the C-term NCOA part of VGLL2-NCOA2 and TEAD1-NCOA2 fusions interacted with CBP/p300 (Figure 4A). Interestingly, our motif enrichment analysis identified CREB motif as specifically enriched among VGLL2-NCOA2 CUT&RUN peaks, but not in YAP^{5SA} peaks (Figure 3E). CREB is a known transcription factor interacting with CBP/p300 (Chrivia et al., 1993), further supporting the notion that VGLL2-NCOA2 and TEAD1-NCOA2 fusion proteins might recruit CBP/p300. In addition, the activity of CBP/p300 has been implicated in several types of human cancers (Waddell et al., 2021; Hogg et al., 2021). Thus, we set out to further examine the interaction between CBP/p300 and the fusion proteins and how it may affect downstream transcriptional activation.

We performed the co-IP analysis in HEK293T cells overexpressing VGLL2-NCOA2, TEAD1-NCOA2, and YAP^{5SA} and demonstrated that VGLL2-NCOA2 and TEAD1-NCOA2, but not YAP^{5SA}, were strongly associated with endogenous p300 proteins (Figure 4B), suggesting the specific engagement of p300 by fusion proteins. To further examine the potential functional regulation of fusion proteins-mediated transcription by CBP/p300, we carried out the CUT&RUN sequencing analysis to map p300 genomic occupancy sites in control and VGLL2-NCOA2- or TEAD1-NCOA2-expressing HEK293T cells (Figure 4C-E). Pathway enrichment analysis of p300 binding peaks annotated by the nearest genes showed significant enrichment of Hippo pathway-related genes in both VGLL2-NCOA2 and TEAD1-NCOA2

expressing cells but not in the control cells (Figure 4C), suggesting that VGLL2-NCOA2 and TEAD1-NCOA2 fusion proteins recruit the CBP/p300 complex to a specific set of genes, likely including the TEAD-dependent downstream target genes. In keeping with this result, our *de novo* motif analysis also revealed that TEAD and AP1 binding sequences were among the top-ranking motifs identified in p300 occupied genomic sites, specifically in VGLL2-NCOA2- and TEAD1-NCOA2-expressing cells (Figure 4D). Interestingly, we noticed that the CREB binding sequence was one of the top-ranking motifs identified in p300 peaks in both control and VGLL2-NCOA2/TEAD1-NCOA2-expressing cells (Figure 4D), consistent with the notion that the CREB family transcription factors are the downstream binding partners of CBP/p300, further validating our CUT&RUN datasets. Upon further examining the binding profiles of p300 in the loci of CTGF, ANKRD1, and CYR61, we showed that p300 bound to these loci in VGLL2-NCOA2/TEAD1-NCOA2-expressing cells, but not in control cells (Figure 4E). More importantly, p300 bound to the same genomic regions that were also occupied by VGLL2-NCOA2 identified in VGLL2-NCOA2 CUT&RUN assay (Figure 3F). As a control, we showed that p300 occupied the genomic sites within the CREB3 locus in cells with or without the expression of the fusion proteins (Figure 4E). Taken together, these data suggest that VGLL2-NCOA2 and TEAD1-NCOA2 fusion proteins interact with CBP/p300, recruiting them to promote TEAD target gene expression.

p300 is required for VGLL2-NCOA2 and TEAD1-NCOA2-induced tumorigenesis.
To test whether VGLL2-NCOA2- and TEAD1-NCOA2-mediated sarcomagenesis is CBP/p300 dependent, we utilized the C2C12 myoblast transformation models both *in vitro* and *in vivo*. Prior reports have demonstrated that VGLL2-NCOA2 can induce oncogenic transformation of C2C12 cells in cell culture and allograft mouse tumor models (Watson et al., 2023). However, it is not known whether VGLL2-NCOA2 or TEAD1-NCOA2 can induce TEAD-mediated transcription and whether p300 is functionally relevant in these models.

We first demonstrated that VGLL2-NCOA2 binds to p300 via its C-terminal NCOA2 part using co-immunoprecipitation assays (Figure 5A), highlighting the essential role of the NCOA2 part of the fusion proteins in recruiting P300 to induce downstream transcription and tumorigenesis. We found that the expression of both VGLL2-NCOA2 and TEAD1-NCOA2 fusion proteins was able to robustly induce the transcription of the known Tead target genes, Ctgf, Ankrd1, and Cyr61, in C2C12 cells (Figure 5B-D). By utilizing a potent p300 small molecule inhibitor, A485, which inhibits CBP/p300 activity both *in vitro* and *in vivo* (Hogg et al., 2021; Lasko et al., 2017), we showed that p300 inhibition by A485 treatment strongly inhibited transcriptional up-regulation of Ctgf, Cyr61, and Ankrd1 induced by the fusion proteins (Figure 5B-D). In contrast, A485 was not able to strongly block YAP^{5SA}-induced Tead target gene expression in C2C12 cells (Figure 5B-D), suggesting that CBP/p300 is required for VGLL2-NCOA2 and TEAD1-NCOA2-dependent gene expression but is largely dispensable for YAP/TAZ-induced target gene transcription. Furthermore, we demonstrated that VGLL2-NCOA2 and TEAD1-NCOA2 were also able to induce colony formation of C2C12 cells in soft agar (Figure 5E). More importantly, A485 treatment markedly reduced the numbers and sizes of the soft agar colonies induced by TEAD1-NCOA2 and VGLL2-NCOA2 but not YAP^{5SA} (Figure 5F and

G), which is consistent with the differential effect of p300 inhibition on downstream gene transcription induced by the fusion proteins or YAP (Figure 5B-D).

To examine the functional dependence of CBP/p300 in tumorigenesis *in vivo*, we took advantage of the C2C12 allograft tumor models and demonstrated that both VGLL2-NCOA2 and TEAD1-NCOA2-expressing C2C12 cells were able to generate aggressive tumors when allografted into nude mice, leading to termination of tumor-bearing mice at around 30 days post-injection. These VGLL2-NCOA2- and TEAD1-NCOA2-expressing tumors were highly proliferative, measured by Ki67 staining, but exhibited heterogeneous expression of Desmin (Figure 6A and B). In addition, we found that p300 inhibition by A485 significantly blocked the tumor growth in both VGLL2-NCOA2 and TEAD1-NCOA2 allograft tumor models (Figure 6C and D), and A485 treatment markedly decreased the proliferation of tumor cells (Figure 6E and F) and the transcription of the target genes, including Ctgf, Cyr61, and Ankrd1 (Figure 6G and H), in both VGLL2-NCOA2 and TEAD1-NCOA2 tumor models. Together, these data, both *in vitro* and *in vivo*, suggest that the CBP/p300 factors are essential for tumorigenesis induced by VGLL2-NCOA2 and TEAD1-NCOA2 fusion proteins.

Discussion

Mis-regulation of YAP and TAZ, including protein upregulation, nuclear accumulation and fusion translocation, has emerged as a major mechanism underlying Hippo signaling involvement in tumorigenesis (Piccolo et al., 2023; Thompson 2020; Franklin et al., 2023; Szulzewsky et al., 2021; Garcia et al., 2022). In this work, our characterization of VGLL2-NCOA2 and TEAD1-NCOA2 fusion proteins generated by recurrent rearrangement in scRMS provides a distinct mechanism of oncogenic transformation that is related to the Hippo pathway but independent of the YAP/TAZ function.

Among the members of the VGLL family proteins, VGLL4 stands out as a *bona fide* transcriptional repressor for YAP/TAZ via its two TEAD-binding TDU domains. The other members of the family, VGLL1-3, contain a single TDU domain, and it is not fully understood whether and how they regulate YAP/TAZ-TEAD transcriptional output. Unlike YAP, TAZ, and VGLL2-NCOA2 fusion, VGLL2 itself does not appear to be a strong activator of TEAD-mediated transcription, even when overexpressed in cells. In both VGLL2-NCOA2 and TEAD1-NCOA2 fusions, the lack of NCOA2 N-terminal domains suggests that they are unlikely to be subject to downstream regulation by nuclear receptors, the canonical binding partners of the NCOA/SRC transcriptional regulators (Yi et al., 2021). Our previous work showed that the NCOA family proteins are associated with the YAP/TAZ-TEAD transcriptional machinery (Liu et al., 2016); however, the presence of YAP/TAZ in the complex appears to be dominant in directing TEAD-mediated transcriptional activation in the normal context. Clearly, the C-terminal NCOA2 TADs render robust transcriptional activity in both VGLL2-NCOA2 and TEAD1-NCOA2 fusions, underlying their oncogenic activity that bypasses the requirement for YAP/TAZ.

Our data showed that VGLL2-NCOA2 and TEAD1-NCOA2 fusions converge on the TEAD family transcription factors or TEAD-mediated genomic occupancy, highlighting the central role of TEAD in Hippo-related tumorigenesis. The small molecule TEAD inhibitors are currently undergoing preclinical or clinical evaluation for cancer treatment (Pobbati et al., 2023). These inhibitors target TEAD auto-palmitoylation, an enzymatic-like activity carried out by the C-terminal YAP/TAZ binding domain of the TEAD proteins (Li et al., 2020; Pobbati et al., 2023; Chan et al., 2016; Holden et al., 2020; Kaneda et al., 2020; Tang et al., 2021; Hu et al., 2022). The lack of YAP/TAZ binding domain in TEAD1 fusion results in the inability of the TEAD palmitoylation inhibitor to suppress gene transcription, suggesting the potential limitation of TEAD palmitoylation inhibitors in tumors carrying TEAD rearrangements. In addition, current TEAD small molecule inhibitors are generally thought to allosterically affect the binding between YAP/TAZ and TEAD. How these inhibitors may affect TEAD interaction with VGLL or VGLL fusion proteins requires further investigation.

Our identification of CBP/p300 as specific epigenetic regulators for VGLL2-NCOA2 and TEAD1-NCOA2 proteins provides a molecular mechanism underlying their YAP/TAZ-independent regulation of transcription and tumorigenesis. In another recurrent VGLL2 rearrangement identified in scRMS, CITED2, the 3' partner in the VGLL2-CITED2 fusion, is a known transcriptional regulator associated with CBP/p300 (Alaggio et al., 2016; Bhattacharya et al., 1999; Bamforth et al., 2001). It is possible that the VGLL2-CITED2 fusion also mediates YAP/TAZ-independent TEAD-dependent transcriptional activation by engaging CBP/p300. Our data using small molecular CBP/p300 inhibitors both *in vitro* and *in vivo* further supports its critical role in VGLL and TEAD fusion protein-mediated oncogenic transformation. This finding may also provide a potential therapeutic strategy for scRMS characterized by these fusion proteins, as well as a range of other tumors carrying NCOA1/2/3 rearrangements, including uterine sarcoma (Niu et al., 2023), mesenchymal chondrosarcoma (Wang et al., 2012; Tanaka et al., 2023), soft tissue angiofibroma (Jin et al., 2012; Yamashita et al., 2023), ovarian sex cord tumors (Goebel et al., 2020; Lu et al., 2023), leukemia (Strehl et al., 2008), colon cancer (Yu et al., 2016), and ependymoma (Tauziède-Espariat et al., 2021; Tomomasa et al., 2021).

Materials and Methods

Key Resources Table

Reagent type (species) or resource	Designation	Source or reference	Identifiers	Additional information
antibody	anti-Flag (mouse monoclonal)	Invitrogen	MA1-91878	CUT&RUN (0.5 µg)
antibody	anti-GAPDH (Rabbit monoclonal)	Cell Signaling Technology	2118	WB (1:10000)
antibody	anti-YAP/TAZ (Rabbit monoclonal)	Cell Signaling Technology	8418	WB (1:1000)
antibody	anti-panTEAD (Rabbit monoclonal)	Cell Signaling Technology	13295	WB (1:1000)
antibody	anti-V5 (Rabbit monoclonal)	Cell Signaling Technology	13202	WB (1:1000)
antibody	anti-p300(Rabbit monoclonal)	Cell Signaling Technology	86377	WB (1:1000); CUT&RUN (0.5 µg)
antibody	anti-Flag(Rabbit monoclonal)	Cell Signaling Technology	2368	WB (1:1000); IP(1:50)
antibody	anti-Flag (mouse monoclonal)	Cell Signaling Technology	F9291	WB (1:1000); IP(1:50)
antibody	anti-HA(Rabbit monoclonal)	Cell Signaling Technology	3724	WB (1:1000); IP(1:50)

antibody	anti-HA(mouse monoclonal)	Cell Signaling Technology	2367	WB (1:1000); IP(1:50)
antibody	HRP-conjugated secondary antibodies	Jackson Laboratories		WB (1:2000)
antibody	anti-Ki67 (Rabbit monoclonal)	Cell Signaling Technology	12202	IHC (1:500)
antibody	anti-Desmin (Rabbit monoclonal)	Cell Signaling Technology	5332	IHC (1:100)
biological sample (Mouse)	Muscle tissue of leg	Shanghai Chest Hoospital		Freshly isolated from nude mouse
cell line (Homo-sapiens)	HEK293T	ATCC	CRL-3216	
cell line (Mouse-sapiens)	C2C12	ATCC	CRL-1772	
chemical compound, drug	A485	SelleckChem	S8740	
chemical compound, drug	streptavidin Sepharose beads	GE Healthcare	17511301	
chemical compound, drug	SignalStain® Antibody Diluent	Cell Signaling Technology	8112	
chemical compound, drug	Lipofectamine 2000	Invitrogen	11668019	
chemical compound, drug	CP1	MCE	HY-139330	
commercial assay or kit	CUTANA™ ChIC/CUT&RUN Kit	EpiCypher	14-1048	

commercial assay or kit	CUT&RUN Library Prep Kit	EpiCypher	14-1001	
commercial assay or kit	RNeasy Mini Kit	Qiagen	74104	
commercial assay or kit	Vectastain Elite ABC kit	Vector Laboratories	PK-6105	
commercial assay or kit	In-Fusion HD Cloning	Clontech	Clontech:639647	
commercial assay or kit	dual-luciferase reporter kit	Promega	E1910	
commercial assay or kit	iTaq Universal One-Step RT-qPCR Kit	BioRad	1725150	
commercial assay or kit	BeyoClick™ EdU Cell Proliferation Kit with Alexa Fluor 488	Beyotime	C0071	
qPCR-based reagent	iTaq Universal One-Step RT-qPCR Kit	BioRad	1725150	
qPCR-based reagent	GAPDH-F'	This paper	PCR primers	GGAGCGAGATCCCTCCAAAAT
qPCR-based reagent	GAPDH-R'	This paper	PCR primers	GGCTGTTGTCATACTTCTCATGG
qPCR-based reagent	CTGF-F'	This paper	PCR primers	CAGCATGGACGTTCGTCTG
qPCR-based reagent	CTGF-R'	This paper	PCR primers	AACCACGGTTTGGTCCTTGG
qPCR-based reagent	ANKRD1-F'	This paper	PCR primers	GCCTACGTTTCTGAAGGCTG
qPCR-based reagent	ANKRD1-R'	This paper	PCR primers	GTGGATTCAAGCATATCACGGA

				A
qPCR-based reagent	CYR61-F'	This paper	PCR primers	CAGGACTGTG AAGATGCGGT
qPCR-based reagent	CYR61-R'	This paper	PCR primers	GCCTGTAGAA GGGAAACGCT
qPCR-based reagent	Actb-F'	This paper	PCR primers	GTGACGTTGAC ATCCGTAAAGA
qPCR-based reagent	Actb-R'	This paper	PCR primers	GCCGGACTCA TCGTACTCC
qPCR-based reagent	Ctgf-F'	This paper	PCR primers	GACCCAACTAT GATGCGAGCC
qPCR-based reagent	Ctgf-R'	This paper	PCR primers	CCCATCCCACA GGTCTTAGAAC
qPCR-based reagent	Ankrd1-F'	This paper	PCR primers	GGATGTGCCG AGGTTTCTGAA
qPCR-based reagent	Ankrd1-R'	This paper	PCR primers	GTCCGTTTATA CTCATCGCAGA C
qPCR-based reagent	Cyr61-F'	This paper	PCR primers	TAAGGTCTGCG CTAAACAACTC
qPCR-based reagent	Cyr61-R'	This paper	PCR primers	CAGATCCCTTT CAGAGCGGT

Cell Lines, Transfection, Lentiviral Infections and Luciferase Reporter Assays

HEK293T (cat. CRL-3216, ATCC, Manassas, VA, USA) and C2C12 (cat. CRL-1772, ATCC) cells were cultured in DMEM supplemented with 10% fetal bovine serum (FBS) and 1% penicillin/streptomycin. Transfection in HEK293T cells was performed using Lipofectamine 2000 (cat. 11668019, Invitrogen, Waltham, MA, USA). For luciferase reporter assays, HEK293T cells were transfected with the luciferase reporter construct TBS-Luc (8XGTIIC-Luc, cat. 34615, Addgene, 8xGTIIC-luc was a gift from Stefano Piccolo), and the expression vectors for YAP^{5SA}, TAZ^{4SA}, VGLL2, NCOA2, TEAD1, TEAD-ENR, VGLL2-NCOA2, VGLL2-$NCOA2^{\Delta VGLL2}$, VGLL2-$NCOA2^{\Delta NCOA2}$, and TEAD1-NCOA2 (generated by and purchased from Genscript, Piscataway, NJ, USA; and GentleGen, Suzhou, Jiangsu Province, China) and pCMV-Renilla luciferase. Luciferase activities were conducted 24 hours after transfection in the cells treated with or without the TEAD inhibitor CP1 (5 μM for 24 hours) using the dual-luciferase reporter kit (cat. E1910, Promega, Madison, WI, USA). Assays were conducted in triplicates and quantified using PerkinElmer EnVision plate reader. For lentiviral

infection, pLKO or pLX based constructs expressing VGLL2-NCOA2, TEAD1-NCOA2, or shRNAs against YAP (5'-CCGGAAGCTTTGAGTTCTGACATCCCTCGAGGGATGTCAGAACTCAAAGCTTTTTTTC-3', cat. 27368, Addgene, pLKO1-shYAP1 was a gift from Kunliang Guan) or TAZ (TRCN0000019470, purchased from Sigma, St. Louis, MO, USA) were transfected along with the packaging plasmids into growing HEK293T cells. Viral supernatants were collected 48 hours after transfection, and target cells were infected in the presence of polybrene and underwent selection with puromycin for 4-5 days. All cell lines used in this study were authenticated by short tandem repeat (STR) profiling and confirmed to be free of Mycoplasma contamination using a Mycoplasma detection assay.

Protein immunoprecipitation and Western blot

Cultured HEK293T cells were lysed in lysis buffer (50 mM Tris-HCl, pH 7.4, 150 mM NaCl, 0.5 mM EDTA, 1% Triton X-100, phosphatase inhibitor cocktail, cOmplete EDTA-free protease inhibitors cocktail) for 30 minutes at 4° C. The supernatants of the extracts were then used for the immunoprecipitation and western blot following the protocols described previously (Cotton et al., 2017). The primary antibodies used in these assays were: GAPDH (cat. 2118, 1:5000, Cell Signaling Technology, Danvers, MA, USA), YAP/TAZ (cat. 8418, 1:1000, Cell Signaling Technology), panTEAD (cat. 13295, 1:1000, Cell Signaling Technology), V5-tag (cat. 13202, 1:1000, Cell Signaling Technology), p300 (cat. 86377, 1:1000, Cell Signaling Technology), Flag-tag (cat. 2368, 1:1000, Cell Signaling Technology and cat. F9291, 1:1000, Sigma), HA-tag (cat. 3724 and cat. 2367, 1:1000, Cell Signaling Technology). HRP-conjugated secondary antibodies used for detection were obtained from Jackson Laboratories (Sacramento, CA, USA).

Quantitative RT-PCR (qPCR)

Total RNA was extracted using the RNeasy Mini Kit (cat. 74104, Qiagen, Germantown, MD, UAS). Gene expression was quantified using the iTaq Universal One-Step RT-qPCR Kit (cat. 1725150, BioRad, Hercules, CA, USA) in Applied Biosystems and normalized to GAPDH or Actb. The primers used in this study are provided in Key Resources Table. qPCR experiments were performed in triplicate, with average cycle threshold (Ct) values from three independent reactions used for analysis.

RNA Sequencing (RNA-seq)

Total RNA was isolated with the RNeasy Mini Kit (cat. 74104, QIAGEN). The integrity of the isolated RNA and RNA-seq libraries was analyzed by Novogene. All libraries had at least 50 million reads sequenced (150 bp paired-end). The correlation between gene expression changes was performed using Pearson correlation analysis. The *p*-values of gene changes in control groups compared with the experimental group were determined by Student's t-test. Plots of correlation between fold change were generated by the ggplot2 package in R. Principal component analysis (PCA) was determined and plotted using the M3C package in R. Gene Set Enrichment Analysis was performed using GSEA software. We performed RNA-seq in triplicate for each condition and each replicate was independently processed and analyzed.

Cleavage under targets and release using nuclease (CUT&RUN)

CUT&RUN was performed using the EpiCypher kit (cat. 14-1048, EpiCypher, Durham, NC, USA). Approximately 0.5 million cells were used for each reaction. In brief, HEK293T cells expressing YAP^{5SA} or VGLL2-NCOA2, or TEAD1-NCOA2 were attached to preactivated ConA beads for 10 minutes at room temperature. Then, 0.5 µg of antibodies against Flag (cat. MA1-91878, Invitrogen) or p300 (cat. 86377, Cell Signaling Technology) as well as control IgG were added to the reactions and incubated overnight at 4° C. The cells were incubated with pAG-MNase for 10 minutes at room temperature prior to activation by calcium chloride. Subsequently, the cells were incubated at 4° C for 2 hours prior to the addition of stop buffer. DNA was purified for library construction using a CUT&RUN Library Prep Kit (cat. 14-1001, EpiCypher). Illumina HiSeq sequencing of approximately 10 million paired-end 150-bp reads was performed at Novogene. MACS2 software (v2.2.7.1) was used for peak calling. Deeptools software (v3.5.1) was used to plot heatmaps of the distribution of reads around TSS. Homer software (v4.11) was used to identify motifs. MANorm2 software (v1.2.0) was used to identify differentially enriched regions between two samples and/or two groups of samples. The scatter plot of the comparison of the two groups of samples is plotted according to the standardized expression mean. The enriched peaks were visualized in IGV (v2.4.10) software. GO and KEGG Pathway analysis were performed based on the promoter enriched peaks associated genes by the ClusterProfiler R packages (v3.18.1). CUT&RUN assays were performed in duplicate for each condition and each replicate was independently processed and analyzed.

Assay for transposase-accessible chromatin (ATAC-seq)

ATAC-seq library construction was performed as previously reported (Buenrostro et al., 2013; Bajic et al., 2018). Briefly, nuclei were extracted from HEK293T cells expressing GFP or VGLL2-NCOA2, and the nuclei pellet was resuspended in the Tn5 transposase reaction mix. The transposition reaction was incubated at 37° C for 30 minutes. Equimolar Adapter 1 and Adapter 2 were added after transposition, and PCR was then performed to amplify the library. After PCR amplification, libraries were purified with AMPure beads. The library was checked with Qubit and real-time PCR for quantification, and bioanalyzer for size distribution detection. Quantified libraries were pooled and sequenced on Illumina platforms, according to the effective library concentration and data amount required. ATAC-seq bioinformatics data analysis was performed following Harvard FAS Informatics ATAC-seq Guidelines. Briefly, Genrich software (v1.30.3) was used for peak calling and blacklist regions were removed. Deeptools software (v3.5.1) was used to plot heatmaps of the distribution of reads around TSS. ChIPseeker R package (v1.30.3) was used to annotate the enriched peaks. Homer software (v4.11) was used to identify motifs. MANorm2 R package was used to perform differentially enriched region analysis between two groups of samples. The scatter plot of the comparison of the two groups of samples is plotted according to the standardized expression mean. GO and KEGG pathway enrichment analysis were performed with ClusterProfiler R package (v3.18.1) based on the enriched peak and differentially enriched region associated genes. ATAC-seq was performed in duplicate for each condition and each replicate was independently processed and analyzed.

BioID proximity ligation and Mass Spectrum analysis

The expression vectors pGIPZ-nlsGFP, pGIPZ-nlsYAP^{5SA}, pGIPZ-nlsTAZ^{4SA}, pGIPZ-VGLL2-NCOA2, and pGIPZ-TEAD1-NCOA2 generated by PCR sub-cloning into the pGIPZ vector were transiently transfected into HEK293T cells. The biotin treatment and BioID pull-down procedures were performed as described previously (Roux et al., 2012). Briefly, 24 hours after transfection, the cells at ~80% confluence were treated with biotin at 50 µM for 24 hours. After washing with cold PBS, the cells were lysed in lysis buffer (50 mM Tris-HCl, pH 7.5, 150 mM NaCl, 1% NP-40, 1 mM EDTA, 1 mM EGTA, 0.1% SDS, 0.5% sodium deoxycholate, 250U of Benzonase, and protease inhibitor), and the cell lysate was incubated at 4° C for 1 hour and sonicated on ice three times. The supernatant was then mixed with pre-washed streptavidin Sepharose beads (cat.17511301, GE Healthcare, Bronx, NY, USA) and incubated at 4° C with rotation for 3 hours. After affinity purification, the agarose beads were washed with lysis buffer followed by two washes with TAP buffer (50mM HEPES-KOH, pH 8.0, 100mM KCl, 10% glycerol, 2mM EDTA, and 0.1% NP-40) and three washes with ABC buffer (50mM Ammonium Bicarbonate, pH 8.0). Protein samples were then eluted by boiling for 5 minutes at 95° C in SDS-containing buffer and collected from SDS-PAGE gels before subjecting to Mass Spectrum analysis. MS data were searched against a protein database (UniProt KB) using the Mascot search engine program (Matrix Science, London, UK) for protein identification. MS data were validated using the Scaffold 4 program (Proteome Software Inc., Portland OR, USA).

Soft agar colony formation and EdU-based proliferation assays

The soft agar colony formation protocol was described in Borowicz et al (Borowicz et al., 2014). Briefly, in a well of a 6-well plate, a bottom layer of 1% agar in growth media (DMEM + 10% FBS) was plated and solidified, followed by a top layer of 0.6% agar + growth media containing 5000 C2C12 cells with or without expressing VGLL2-NCOA2 or TEAD1-NCOA2. A485 (cat. S8740, SelleckChem, Houston, TX, USA) was dissolved in DMSO to prepare 5 mM stock solution. 1 ml of growth media with or without A485 (5 µM working concentration) was added to the top of each well and replenished every 2−3 days. Colony growth was monitored under a microscope for 2 weeks. Colonies from each group were imaged using a Zeiss Axio Photo Observer microscope. Eight colonies from each group were randomly selected for size measurement, and the diameter of each colony was measured using ZEN 3.2 blue edition software. Colony numbers were counted from three random fields of view and representative images were shown.

Cell proliferation was assessed using the BeyoClick™ EdU Cell Proliferation Kit with Alexa Fluor 488 (Beyotime, C0071) according to the manufacturer's protocol. Briefly, cells were incubated with 10 µM EdU for 120 minutes, followed by digestion with 0.25% trypsin-EDTA. The cells were then fixed in 4% paraformaldehyde (PFA) and permeabilized with PBS containing 0.3% Triton X-100 at room temperature for 15 minutes. After three washes with PBS containing 3% BSA, a click reaction solution was added and incubated at room temperature for 30 minutes, followed by Hoechst 33342 counterstaining. Edu detection assays were performed in triplicate and representative images were shown.

Mouse allograft experiments and tumor processing

All animal protocols and procedures were approved by the institutional animal care and use committees at the Shanghai Chest Hospital and the University of Massachusetts Chan Medical School. Nude mice were purchased from The Jackson Laboratory (Male, 3-4 weeks, Nu/J, cat. 002019, Shanghai, China). Nude mice were randomly divided into groups. C2C12-control, C2C12-VGLL2-NCOA2, and C2C12-TEAD1-NCOA2 cell lines were utilized in allograft experiments adapted from Watson et al (Watson et al., 2023). Five million cells were resuspended in 100 µL of sterile PBS and injected intramuscularly into the leg of nude mice under anesthesia. Each experimental group had six mice and mouse legs were assessed five days after initial injection. Based on the weight of each mouse, an appropriate volume of the A485 stock solution (5mM in DMSO) was diluted in 500 µL saline and then administered daily via intraperitoneal injection at a dose of 100 mg/kg (Lasko et al., 2017). The height and width of the injected legs were measured using calipers to calculate the volume until 30 days post-injection (initial leg volume was 50−80 mm^3). Tumor tissue was snap-frozen in liquid nitrogen, and RNA was isolated with Trizol for qPCR analysis. For immunohistochemistry (IHC), tumors were fixed in a 4% paraformaldehyde solution and mounted in paraffin blocks for microtome sectioning.

Immunohistochemistry

Sections were deparaffinized and rehydrated before undergoing heat-induced antigen retrieval in 10 mM sodium citrate buffer (pH 6.0, Solarbio, cat. C1013) for 30 minutes. Slides were blocked for endogenous peroxidase for 20 minutes, then blocked for 1 hour in 5% BSA, 1% goat serum, 0.1% Tween-20 buffer in PBS, and incubated overnight at 4° C with the primary antibody diluted in blocking buffer or SignalStain® Antibody Diluent (cat. 8112, Cell Signaling Technology). Slides were incubated with biotinylated secondary antibodies for 1 hour at room temperature, and the signal was detected using the Vectastain Elite ABC kit (cat. PK-6105, Vector Laboratories, Newark, CA, USA). Hematoxylin was used for counterstaining in IHC. Antibodies and dilutions used in the studies: Ki67 (cat. 12202, 1:500, Cell Signaling Technology), Desmin (cat. 5332, 1:100, Cell Signaling Technology).

Statistics and reproducibility

Statistical analyses were performed using GraphPad Prism 8 software or R. The repetition of the experiment is shown in the figures and corresponding figure legends. The results were expressed as the mean ± SEM. Statistical significance was determined using a one-way ANOVA test for most datasets. The Student's t-test was used when comparing two groups.

Data Availability

The data generated in this study are publicly available in Gene Expression Omnibus (GEO) at GSE260781, GSE260782, and GSE260783.

Ethics statement

All animal protocols and procedures were approved by the animal ethics committee at the Shanghai Chest Hospital (reference numbers: KS(Y)24388).

Acknowledgments

This work was supported by grants from the National Institutes of Health (R01DK127207 and R01DK127180 to J.M., R01CA238270 to X.W. and J.M.), the National Natural Science Foundation of China (82173015 to J.W.). We also thank the members of the Wang lab and Mao lab for their helpful discussions.

Impact Statement

VGLL2 fusion proteins identified in sarcoma patients drive Hippo signaling-independent transcriptional programs and tumor development.

Disclosure and competing interests statement

Dr. Xu Wu has a financial interest in Tasca Therapeutics, which is developing small molecule modulators of TEAD palmitoylation and transcription factors. Dr. Wu's interests were reviewed and are managed by Mass General Hospital, and Mass General Brigham in accordance with their conflict of interest polices.

References

Alaggio R, Zhang L, Sung YS, Huang SC, Chen CL, Bisogno G, Zin A, Agaram NP, LaQuaglia MP, Wexler LH, Antonescu CR. 2016. A Molecular Study of Pediatric Spindle and Sclerosing Rhabdomyosarcoma: Identification of Novel and Recurrent Vgll2-Related Fusions in Infantile Cases. *Am J Surg Pathol* **40**: 224-35. DOI: https://dx.doi.org/10.1097/pas.0000000000000538, PMID: 26501226

Bajic M, Maher KA, Deal RB. 2018. Identification of Open Chromatin Regions in Plant Genomes Using Atac-Seq. *Methods Mol Biol* **1675**: 183-201. DOI: https://dx.doi.org/10.1007/978-1-4939-7318-7_12, PMID: 29052193

Bamforth SD, Bragança J, Eloranta JJ, Murdoch JN, Marques FI, Kranc KR, Farza H, Henderson DJ, Hurst HC, Bhattacharya S. 2001. Cardiac Malformations, Adrenal Agenesis, Neural Crest Defects and Exencephaly in Mice Lacking Cited2, a New Tfap2 Co-Activator. *Nat Genet* **29**: 469-74. DOI: https://dx.doi.org/10.1038/ng768, PMID: 11694877

Bannister AJ, Kouzarides T. 1996. The Cbp Co-Activator Is a Histone Acetyltransferase. *Nature* **6610**: 641-3. DOI: https://dx.doi.org/10.1038/384641a0, PMID: 8967953

Bhattacharya S, Michels CL, Leung MK, Arany ZP, Kung AL, Livingston DM. 1999. Functional Role of P35srj, a Novel P300/Cbp Binding Protein, During Transactivation by Hif-1. *Genes Dev* **13**: 64-75. DOI: https://dx.doi.org/10.1101/gad.13.1.64, PMID: 9887100

Borowicz S, Van Scoyk M, Avasarala S, Karuppusamy Rathinam MK, Tauler J, Bikkavilli RK, Winn RA. 2014. The Soft Agar Colony Formation Assay. *J Vis Exp* **92**: e51998. DOI: https://dx.doi.org/10.3791/51998, PMID: 25408172

Buenrostro JD, Giresi PG, Zaba LC, Chang HY, Greenleaf WJ. 2013. Transposition of Native Chromatin for Fast and Sensitive Epigenomic Profiling of Open Chromatin, DNA-Binding Proteins and Nucleosome Position. *Nat Methods* **10**: 1213-8. DOI: https://dx.doi.org/10.1038/nmeth.2688, PMID: 24097267

Cai J, Choi K, Li H, Pulgar Prieto KD, Zheng Y, Pan D. 2022. Yap-Vgll4 Antagonism Defines the Major Physiological Function of the Hippo Signaling Effector Yap. *Genes Dev* **36**: 1119-28. DOI: https://dx.doi.org/10.1101/gad.350127.122, PMID: 36522128

Calses PC, Crawford JJ, Lill JR, Dey A. 2019. Hippo Pathway in Cancer: Aberrant Regulation and Therapeutic Opportunities. *Trends Cancer* **5**: 297-307. DOI: https://dx.doi.org/10.1016/j.trecan.2019.04.001, PMID: 31174842

Chan P, Han X, Zheng B, DeRan M, Yu J, Jarugumilli GK, Deng H, Pan D, Luo X, Wu X. 2016. Autopalmitoylation of Tead Proteins Regulates Transcriptional Output of the Hippo Pathway. *Nat Chem Biol* **12**: 282-9. DOI: https://dx.doi.org/10.1038/nchembio.2036, PMID: 26900866

Chen S, Rudzinski ER, Arnold MA. 2020. Challenges in the Diagnosis of Pediatric Spindle Cell/Sclerosing Rhabdomyosarcoma. *Surg Pathol Clin* **13**: 729-38. DOI: https://dx.doi.org/10.1016/j.path.2020.08.010, PMID: 33183730

Chrivia JC, Kwok RP, Lamb N, Hagiwara M, Montminy MR, Goodman RH. 1993. Phosphorylated Creb Binds Specifically to the Nuclear Protein Cbp. *Nature* **365**: 855-9. DOI: https://dx.doi.org/10.1038/365855a0, PMID: 8413673

Cotton JL, Li Q, Ma L, Park JS, Wang J, Ou J, Zhu LJ, Ip YT, Johnson RL, Mao J. 2017. Yap/Taz and Hedgehog Coordinate Growth and Patterning in Gastrointestinal Mesenchyme. *Dev Cell* **43**: 35-47.e4. DOI: https://dx.doi.org/10.1016/j.devcel.2017.08.019, PMID: 28943241

Cyrta J, Gauthier A, Karanian M, Vieira AF, Cardoen L, Jehanno N, Bouvet M, Bouvier C, Komuta M, Le Loarer F, Orbach D, Rome A, Minard-Colin V, Brichard B, Pluchart C, Thebaud E, Renard M, Pannier S, Brisse H, Petit P, et al. 2021. Infantile Rhabdomyosarcomas with Vgll2 Rearrangement Are Not Always an Indolent Disease: A Study of 4 Aggressive Cases with Clinical, Pathologic, Molecular, Radiologic Findings. *Am J Surg Pathol* **45**: 854-67. DOI: https://dx.doi.org/10.1097/pas.0000000000001702, PMID: 33949344

Driskill JH, Zheng Y, Wu BK, Wang L, Cai J, Rakheja D, Dellinger M, Pan D. 2021. Wwtr1(Taz)-Camta1 Reprograms Endothelial Cells to Drive Epithelioid Hemangioendothelioma. *Genes Dev* **35**: 495-511. DOI: https://dx.doi.org/10.1101/gad.348221.120, PMID: 33766984

Dupont S, Morsut L, Aragona M, Enzo E, Giulitti S, Cordenonsi M, Zanconato F, Le Digabel J, Forcato M, Bicciato S, Elvassore N, Piccolo S. 2011. Role of Yap/Taz in Mechanotransduction. *Nature* **474**: 179-83. DOI: https://dx.doi.org/10.1038/nature10137, PMID: 21654799

Faucheux C, Naye F, Tréguer K, Fédou S, Thiébaud P, Théze N. 2010. Vestigial Like Gene Family Expression in Xenopus: Common and Divergent Features with Other Vertebrates. *Int J Dev Biol* **54**: 1375-82. DOI: https://dx.doi.org/10.1387/ijdb.103080cf, PMID: 20712000

Franklin JM, Wu Z, Guan KL. 2023. Insights into Recent Findings and Clinical Application of Yap and Taz in Cancer. *Nat Rev Cancer* **23**: 512-25. DOI: https://dx.doi.org/10.1038/s41568-023-00579-1, PMID: 37308716

Garcia K, Gingras AC, Harvey KF, Tanas MR. 2022. Taz/Yap Fusion Proteins: Mechanistic Insights and Therapeutic Opportunities. *Trends Cancer* **8**: 1033-45. DOI: https://dx.doi.org/10.1016/j.trecan.2022.08.002, PMID: 36096997

Goebel EA, Hernandez Bonilla S, Dong F, Dickson BC, Hoang LN, Hardisson D, Lacambra MD, Lu FI, Fletcher CDM, Crum CP, Antonescu CR, Nucci MR, Kolin DL. 2020. Uterine Tumor Resembling Ovarian Sex Cord Tumor. Utrosct): A Morphologic and Molecular Study of 26 Cases Confirms Recurrent Ncoa1-3 Rearrangement. *Am J Surg Pathol* **44**: 30-42. DOI: https://dx.doi.org/10.1097/pas.0000000000001348, PMID: 31464709

Hogg SJ, Motorna O, Cluse LA, Johanson TM, Coughlan HD, Raviram R, Myers RM, Costacurta M, Todorovski I, Pijpers L, Bjelosevic S, Williams T, Huskins SN, Kearney CJ, Devlin JR, Fan Z, Jabbari JS, Martin BP, Fareh M, Kelly MJ, et al. 2021. Targeting Histone Acetylation Dynamics and Oncogenic Transcription by Catalytic P300/Cbp Inhibition. *Mol Cell* **81**: 2183-200.e13. DOI: https://dx.doi.org/10.1016/j.molcel.2021.04.015, PMID: 34019788

Holden JK, Crawford JJ, Noland CL, Schmidt S, Zbieg JR, Lacap JA, Zang R, Miller GM, Zhang Y, Beroza P, Reja R, Lee W, Tom JYK, Fong R, Steffek M, Clausen S, Hagenbeek TJ, Hu T, Zhou Z, Shen HC, Cunningham CN. 2020. Small Molecule Dysregulation of Tead Lipidation Induces a Dominant-Negative Inhibition of Hippo Pathway Signaling. *Cell Rep* **31**: 107809. DOI: https://dx.doi.org/10.1016/j.celrep.2020.107809, PMID: 32579935

Hu L, Sun Y, Liu S, Erb H, Singh A, Mao J, Luo X, Wu X. 2022. Discovery of a New Class of Reversible Tea Domain Transcription Factor Inhibitors with a Novel Binding Mode. *Elife* **11**. DOI: https://dx.doi.org/10.7554/eLife.80210, PMID: 36398861

Jin Y, Möller E, Nord KH, Mandahl N, Von Steyern FV, Domanski HA, Mariño-Enríquez A, Magnusson L, Nilsson J, Sciot R, Fletcher CD, Debiec-Rychter M, Mertens F. 2012. Fusion of the Ahrr and Ncoa2 Genes through a Recurrent Translocation T(5;8)(P15;Q13) in Soft Tissue Angiofibroma Results in Upregulation of Aryl Hydrocarbon Receptor Target Genes. *Genes Chromosomes Cancer* **51**: 510-20. DOI: https://dx.doi.org/10.1002/gcc.21939, PMID: 22337624

Kaneda A, Seike T, Danjo T, Nakajima T, Otsubo N, Yamaguchi D, Tsuji Y, Hamaguchi K, Yasunaga M, Nishiya Y, Suzuki M, Saito JI, Yatsunami R, Nakamura S, Sekido Y, Mori K. 2020. The Novel Potent Tead Inhibitor, K-975, Inhibits Yap1/Taz-Tead Protein-Protein Interactions and Exerts an Anti-Tumor Effect on Malignant Pleural Mesothelioma. *Am J Cancer Res* **10**: 4399-415, PMID: 33415007

Kim DI and Roux KJ. 2016. Filling the Void: Proximity-Based Labeling of Proteins in Living Cells. *Trends Cell Biol* **26**: 804-17. DOI: https://dx.doi.org/10.1016/j.tcb.2016.09.004, PMID: 27667171

Koontz LM, Liu-Chittenden Y, Yin F, Zheng Y, Yu J, Huang B, Chen Q, Wu S, Pan D. 2013. The Hippo Effector Yorkie Controls Normal Tissue Growth by Antagonizing Scalloped-Mediated Default Repression. *Dev Cell* **25**: 388-401. DOI: https://dx.doi.org/10.1016/j.devcel.2013.04.021, PMID: 23725764

Kulkarni A, Chang MT, Vissers JHA, Dey A, Harvey KF. 2020. The Hippo Pathway as a Driver of Select Human Cancers. *Trends Cancer* **6**: 781-96. DOI: https://dx.doi.org/10.1016/j.trecan.2020.04.004, PMID: 32446746

Lasko LM, Jakob CG, Edalji RP, Qiu W, Montgomery D, Digiammarino EL, Hansen TM, Risi RM, Frey R, Manaves V, Shaw B, Algire M, Hessler P, Lam LT, Uziel T, Faivre E, Ferguson D, Buchanan FG, Martin RL, Torrent M, et al. 2017. Discovery of a Selective Catalytic P300/Cbp Inhibitor That Targets Lineage-Specific Tumours. *Nature* **550**: 128-32. DOI: https://dx.doi.org/10.1038/nature24028, PMID: 28953875

Li F, Liu R, Negi V, Yang P, Lee J, Jagannathan R, Moulik M, Yechoor VK. 2023. Vgll4 and Menin Function as Tead1 Corepressors to Block Pancreatic Β Cell Proliferation. *Cell Rep* **42**: 111904. DOI: https://dx.doi.org/10.1016/j.celrep.2022.111904, PMID: 36662616

Li Q, Sun Y, Jarugumilli GK, Liu S, Dang K, Cotton JL, Xiol J, Chan PY, DeRan M, Ma L, Li R, Zhu LJ, Li JH, Leiter AB, Ip YT, Camargo FD, Luo X, Johnson RL, Wu X, Mao J. 2020. Lats1/2 Sustain Intestinal Stem Cells and Wnt Activation through Tead-Dependent and Independent Transcription. *Cell Stem Cell* **26**: 675-92.e8. DOI: https://dx.doi.org/10.1016/j.stem.2020.03.002, PMID: 32259481

Liu X, Li H, Rajurkar M, Li Q, Cotton JL, Ou J, Zhu LJ, Goel HL, Mercurio AM, Park JS, Davis RJ, Mao J. 2016. Tead and Ap1 Coordinate Transcription and Motility. *Cell Rep* **14**: 1169-80. DOI: https://dx.doi.org/10.1016/j.celrep.2015.12.104, PMID: 26832411

Lu B, Xia Y, Chen J, Tang J, Shao Y, Yu W. 2023. Ncoa1/2/3 Rearrangements in Uterine Tumor Resembling Ovarian Sex Cord Tumor: A Clinicopathological and Molecular Study of 18 Cases. *Hum Pathol* **135**: 65-75. DOI: https://dx.doi.org/10.1016/j.humpath.2023.01.001, PMID: 36646185

Ma S, Meng Z, Chen R, Guan KL. 2019. The Hippo Pathway: Biology and Pathophysiology. *Annu Rev Biochem* **88**: 577-604. DOI: https://dx.doi.org/10.1146/annurev-biochem-013118-111829, PMID: 30566373

Merritt N, Garcia K, Rajendran D, Lin ZY, Zhang X, Mitchell KA, Borcherding N, Fullenkamp C, Chimenti MS, Gingras AC, Harvey KF, Tanas MR. 2021. Taz-Camta1 and Yap-Tfe3 Alter the Taz/Yap Transcriptome by Recruiting the Atac Histone Acetyltransferase Complex. *Elife* **10**. DOI: https://dx.doi.org/10.7554/eLife.62857, PMID: 33913810

Niu S, Rivera-Colon G, Lucas E. 2023. Aggressive High-Grade Uterine Sarcoma Harboring Meis1-Ncoa2 Fusion and Amplification of Multiple 12q13-15 Genes: A Case Report with Morphologic, Immunohistochemical, Molecular Analysis. *Int J Gynecol Pathol* **42**: 460-65. DOI: https://dx.doi.org/10.1097/pgp.0000000000000937, PMID: 36811835

Ogryzko VV, Schiltz RL, Russanova V, Howard BH, Nakatani Y. 1996. The Transcriptional Coactivators P300 and Cbp Are Histone Acetyltransferases. *Cell* **87**: 953-9. DOI: https://dx.doi.org/10.1016/s0092-8674(00)82001-2, PMID: 8945521

Piccolo S, Panciera T, Contessotto P, Cordenonsi M. 2023. Yap/Taz as Master Regulators in Cancer: Modulation, Function and Therapeutic Approaches. *Nat Cancer* **4**: 9-26. DOI: https://dx.doi.org/10.1038/s43018-022-00473-z, PMID: 36564601

Pobbati AV, Chan SW, Lee I, Song H, Hong W. 2012. Structural and Functional Similarity between the Vgll1-Tead and the Yap-Tead Complexes. *Structure* **20**: 1135-40. DOI: https://dx.doi.org/10.1016/j.str.2012.04.004, PMID: 22632831

Pobbati AV, Kumar R, Rubin BP, Hong W. 2023. Therapeutic Targeting of Tead Transcription Factors in Cancer. *Trends Biochem Sci* **48**: 450-62. DOI: https://dx.doi.org/10.1016/j.tibs.2022.12.005, PMID: 36709077

Roux KJ, Kim DI, Raida M, Burke B. 2012. A Promiscuous Biotin Ligase Fusion Protein Identifies Proximal and Interacting Proteins in Mammalian Cells. *J Cell Biol* **196**: 801-10. DOI: https://dx.doi.org/10.1083/jcb.201112098, PMID: 22412018

Seavey CN, Pobbati AV, Hallett A, Ma S, Reynolds JP, Kanai R, Lamar JM, Rubin BP. 2021. Wwtr1(Taz)-Camta1 Gene Fusion Is Sufficient to Dysregulate Yap/Taz Signaling and Drive Epithelioid Hemangioendothelioma Tumorigenesis. *Genes Dev* **35**: 512-27. DOI: https://dx.doi.org/10.1101/gad.348220.120, PMID: 33766982

Simon E, Faucheux C, Zider A, Thézé N, Thiébaud P. 2016. From Vestigial to Vestigial-Like: The Drosophila Gene That Has Taken Wing. *Dev Genes Evol* **226**: 297-315. DOI: https://dx.doi.org/10.1007/s00427-016-0546-3, PMID: 27116603

Strehl S, Nebral K, König M, Harbott J, Strobl H, Ratei R, Struski S, Bielorai B, Lessard M, Zimmermann M, Haas OA, Izraeli S. 2008. Etv6-Ncoa2: A Novel Fusion Gene in Acute Leukemia Associated with Coexpression of T-Lymphoid and Myeloid Markers and Frequent Notch1 Mutations. *Clin Cancer Res* **14**: 977-83. DOI: https://dx.doi.org/10.1158/1078-0432.Ccr-07-4022, PMID: 18281529

Sun Y, Hu L, Tao Z, Jarugumilli GK, Erb H, Singh A, Li Q, Cotton JL, Greninger P, Egan RK, Ip YT, Benes CH, Che J, Mao J, Wu X. 2022. Pharmacological Blockade of Tead-Yap Reveals Its Therapeutic Limitation in Cancer Cells. *Nat Commun* **13**: 6744. DOI: https://dx.doi.org/10.1038/s41467-022-34559-0, PMID: 36347861

Szulzewsky F, Arora S, Arakaki AKS, Sievers P, Almiron Bonnin DA, Paddison PJ, Sahm F, Cimino PJ, Gujral TS, Holland EC. 2022. Both Yap1-Maml2 and Constitutively Active Yap1 Drive the Formation of Tumors That Resemble Nf2 Mutant Meningiomas in Mice. *Genes Dev* **36**: 857-70. DOI: https://dx.doi.org/10.1101/gad.349876.122, PMID: 36008139

Szulzewsky F, Holland EC, Vasioukhin V. 2021. Yap1 and Its Fusion Proteins in Cancer Initiation, Progression and Therapeutic Resistance. *Dev Biol* **475**: 205-21. DOI: https://dx.doi.org/10.1016/j.ydbio.2020.12.018, PMID: 33428889

Tan G Z L, Saminathan S N, Chang K T E, Odoño E G, Kuick C H, Chen H, Lee V K M. 2020. A Rare Case of Congenital Spindle Cell Rhabdomyosarcoma with Tead1-Ncoa2 Fusion: A Subset of Spindle Cell Rhabdomyosarcoma with Indolent Behavior. *Pathol Int* **70**: 234-36. DOI: https://dx.doi.org/10.1111/pin.12908, PMID: 31999033

Tanaka M, Homme M, Teramura Y, Kumegawa K, Yamazaki Y, Yamashita K, Osato M, Maruyama R, Nakamura T. 2023. Hey1-Ncoa2 Expression Modulates Chondrogenic Differentiation and Induces Mesenchymal Chondrosarcoma in Mice. *JCI Insight* **8**. DOI: https://dx.doi.org/10.1172/jci.insight.160279, PMID: 37212282

Tang T T, Konradi A W, Feng Y, Peng X, Ma M, Li J, Yu F X, Guan K L, Post L. 2021. Small Molecule Inhibitors of Tead Auto-Palmitoylation Selectively Inhibit Proliferation and Tumor Growth of Nf2-Deficient Mesothelioma. *Mol Cancer Ther* **20**: 986-98. DOI: https://dx.doi.org/10.1158/1535-7163.Mct-20-0717, PMID: 33850002

Tauziède-Espariat A, Siegfried A, Nicaise Y, Kergrohen T, Sievers P, Vasiljevic A, Roux A, Dezamis E, Benevello C, Machet M C, Michalak S, Puiseux C, Llamas-Gutierrez F, Leblond P, Bourdeaut F, Grill J, Dufour C, Guerrini-Rousseau L, Abbou S, Dangouloff-Ros V, et al. 2021. Supratentorial Non-Rela, Zfta-Fused Ependymomas: A Comprehensive Phenotype Genotype Correlation Highlighting the Number of Zinc Fingers in Zfta-Ncoa1/2 Fusions. *Acta Neuropathol Commun* **9**: 135. DOI: https://dx.doi.org/10.1186/s40478-021-01238-y, PMID: 34389065

Thompson B J. 2020. Yap/Taz: Drivers of Tumor Growth, Metastasis, Resistance to Therapy. *Bioessays* **42**: e1900162. DOI: https://dx.doi.org/10.1002/bies.201900162, PMID: 32128850

Tomomasa R, Arai Y, Kawabata-Iwakawa R, Fukuoka K, Nakano Y, Hama N, Nakata S, Suzuki N, Ishi Y, Tanaka S, Takahashi J A, Yuba Y, Shiota M, Natsume A, Kurimoto M, Shiba Y, Aoki M, Nabeshima K, Enomoto T, Inoue T, et al. 2021. Ependymoma-Like Tumor with Mesenchymal Differentiation Harboring C11orf95-Ncoa1/2 or -Rela Fusion: A Hitherto Unclassified Tumor Related to Ependymoma. *Brain Pathol* **31**: e12943. DOI: https://dx.doi.org/10.1111/bpa.12943, PMID: 33576087

Totaro A, Panciera T, Piccolo S. 2018. Yap/Taz Upstream Signals and Downstream Responses. *Nat Cell Biol* **20**: 888-99. DOI: https://dx.doi.org/10.1038/s41556-018-0142-z, PMID: 30050119

Waddell A R, Huang H, Liao D. 2021. Cbp/P300: Critical Co-Activators for Nuclear Steroid Hormone Receptors and Emerging Therapeutic Targets in Prostate and Breast Cancers. *Cancers (Basel)* **13**. DOI: https://dx.doi.org/10.3390/cancers13122872, PMID: 34201346

Wang L, Motoi T, Khanin R, Olshen A, Mertens F, Bridge J, Dal Cin P, Antonescu C R, Singer S, Hameed M, Bovee J V, Hogendoorn P C, Socci N, Ladanyi M. 2012. Identification of a Novel, Recurrent Hey1-Ncoa2 Fusion in Mesenchymal Chondrosarcoma Based on a Genome-Wide Screen of Exon-Level Expression Data. *Genes Chromosomes Cancer* **51**: 127-39. DOI: https://dx.doi.org/10.1002/gcc.20937, PMID: 22034177

Watson S, LaVigne C A, Xu L, Surdez D, Cyrta J, Calderon D, Cannon M V, Kent M R, Silvius K M, Kucinski J P, Harrison E N, Murchison W, Rakheja D, Tirode F, Delattre O, Amatruda J F, Kendall G C. 2023. Vgll2-Ncoa2 Leverages Developmental Programs for Pediatric Sarcomagenesis. *Cell Rep* **42**: 112013. DOI: https://dx.doi.org/10.1016/j.celrep.2023.112013, PMID: 36656711

Whittle S, Venkatramani R, Schönstein A, Pack S D, Alaggio R, Vokuhl C, Rudzinski E R, Wulf A L, Zin A, Gruver J R, Arnold M A, Merks J H M, Hettmer S, Koscielniak E, Barr F G, Hawkins D S, Bisogno G, Sparber-Sauer M. 2022. Congenital Spindle Cell Rhabdomyosarcoma: An International Cooperative Analysis. *Eur J Cancer* **168**: 56-64. DOI: https://dx.doi.org/10.1016/j.ejca.2022.03.022, PMID: 35452896

Yamaguchi N. 2020. Multiple Roles of Vestigial-Like Family Members in Tumor Development. *Front Oncol* **10**: 1266. DOI: https://dx.doi.org/10.3389/fonc.2020.01266, PMID: 32793503

Yamashita K, Baba S, Togashi Y, Dobashi A, Ae K, Matsumoto S, Tanaka M, Nakamura T, Takeuchi K. 2023. Clinicopathologic and Genetic Characterization of Angiofibroma of Soft Tissue: A Study of 12 Cases Including Two Cases with Ahrr::Ncoa3 Gene Fusion. *Histopathology* **83**: 57-66. DOI: https://dx.doi.org/10.1111/his.14899, PMID: 36860189

Yi P, Yu X, Wang Z, O'Malley B W. 2021. Steroid Receptor-Coregulator Transcriptional Complexes: New Insights from Cryoem. *Essays Biochem* **65**: 857-66. DOI: https://dx.doi.org/10.1042/ebc20210019, PMID: 34061186

Yu J, Wu W K, Liang Q, Zhang N, He J, Li X, Zhang X, Xu L, Chan M T, Ng S S, Sung J J. 2016. Disruption of Ncoa2 by Recurrent Fusion with Lactb2 in Colorectal Cancer. *Oncogene* **35**: 187-95. DOI: https://dx.doi.org/10.1038/onc.2015.72, PMID: 25823027

Zanconato F, Forcato M, Battilana G, Azzolin L, Quaranta E, Bodega B, Rosato A, Bicciato S, Cordenonsi M, Piccolo S. 2015. Genome-Wide Association between Yap/Taz/Tead And ap-1

at Enhancers Drives Oncogenic Growth. *Nat Cell Biol* **17**: 1218-27. DOI: https://dx.doi.org/10.1038/ncb3216, PMID: 26258633

Zhang W, Gao Y, Li P, Shi Z, Guo T, Li F, Han X, Feng Y, Zheng C, Wang Z, Li F, Chen H, Zhou Z, Zhang L, Ji H. 2014. Vgll4 Functions as a New Tumor Suppressor in Lung Cancer by Negatively Regulating the Yap-Tead Transcriptional Complex. *Cell Res* **24**: 331-43. DOI: https://dx.doi.org/10.1038/cr.2014.10, PMID: 24458094

Zhao B, Li L, Tumaneng K, Wang C Y, Guan K L. 2010. A Coordinated Phosphorylation by Lats and Ck1 Regulates Yap Stability through Scf (Beta-Trcp). *Genes Dev* **24**: 72-85. DOI: https://dx.doi.org/10.1101/gad.1843810, PMID: 20048001

Zheng Y and Pan D. 2019. The Hippo Signaling Pathway in Development and Disease. *Dev Cell* **50**: 264-82. DOI: https://dx.doi.org/10.1016/j.devcel.2019.06.003, PMID: 31386861

Figure Legend

Figure 1. VGLL2-NCOA2 and TEAD1-NCOA2 Induce TEAD-Mediated Transcriptional Activation.

A. Schematic representation of protein structure of VGLL2, TEAD1, NCOA2, VGLL2-NCOA2 and TEAD1-NCOA2. Tondu motif (TDU), TEA DNA binding domain (TEA), YAP binding domain (YBD), basic Helix-Loop-Helix (bHLH), Per-Arnt-Sim domain (PAS), nuclear receptor interaction domain (NID), transcriptional activation domain (TAD). Arrows point to the break points.

B. Immunoblot analysis of YAP^{5SA}, VGLL2-NCOA2, TEAD1-NCOA2, TAZ^{4SA}, TEAD1, VGLL2 and NCOA2 in HEK293T cells transfected with the expression constructs carrying the HA tag. The figure shows the representative results of three biological replicates.

C. YAP^{5SA}, VGLL2-NCOA2, TEAD1-NCOA2, TAZ^{4SA}, TEAD1, VGLL2, and NCOA2 induce transcriptional activation of TBS (TEAD binding site)-luciferase reporter (TBS-Luc) in HEK293T cells. n = 3. ****, $p < 0.0001$.

D. Heatmap showing expression levels of the core genes including CTGF, CYR61, ANKRD1 and AMOTL2 significantly regulated in HEK293T cells expressing YAP^{5SA}, VGLL2-NCOA2 and TEAD1-NCOA2. n=3

E. mRNA levels of CTGF, ANKRD1 and CYR61 in HEK293T cells expressing YAP^{5SA}, VGLL2-NCOA2, TEAD1-NCOA2, TEAD1, VGLL2 or NCOA2. n=3; ****, $p < 0.0001$. NS, no significance.

Figure 2. VGLL2-NCOA2 and TEAD1-NCOA2-induced transcription does not require YAP and TAZ.

A. Co-IP assay showing VGLL2-NCOA2 binding to TEAD1 but not YAP^{5SA}. YAP^{5SA}-Flag or TEAD1-Flag was co-expressed with VGLL2-NCOA2-HA in HEK293T cells and immunoprecipitated with an anti-HA antibody.

B. VGLL2-NCOA2 binds to endogenous TEAD but not YAP/TAZ. Endogenous YAP/TAZ and TEAD proteins in HEK293T cells were detected by anti-YAP/TAZ and panTEAD antibodies, respectively.

C. Co-IP assay showing endogenous YAP/TAZ binding to TEAD1 but not TEAD1-NCOA2. TEAD1-Flag or TEAD1-NCOA2-Flag was expressed in HEK293T cells and immunoprecipitated with an anti-Flag antibody. Endogenous YAP/TAZ proteins were detected by anti-YAP/TAZ antibodies.

D. The activity of TBS-Luc reporter in HEK293T cells expressing YAP^{5SA}, VGLL2-NCOA2, or TEAD1-NCOA2, with TEAD inhibitor CP1 (5 μM) treatment or co-expression of TEAD-ENR repressor construct. n=3; ****, $p < 0.0001$. NS, no significance.

E. Schematic representation of TEAD-ENR. TEA DNA-binding domain (TEA) and Engrailed repressor domain (ENR).
F. Immunoblot analysis of TEAD-ENR expression in HEK293T cells.
G. Co-IP assay showing YAP/TAZ were not essential for VGLL2-NCOA2 binding to endogenous TEAD. VGLL2-NCOA2-HA was expressed in HEK293T cells with or without YAP/TAZ knockdown and immunoprecipitated with an anti-HA antibody.
H. Relative mRNA levels of CTGF, ANKRD1, and CYR61 in HEK293T cells with YAP/TAZ knockdown and expressing VGLL2-NCOA2 or TEAD1-NCOA2. n=3; ****, $p < 0.0001$.

Figure 3. Characterization of VGLL2-NCOA2- and YAP- controlled transcriptional and chromatin landscapes.
A. Intersection of ATAC-seq (n=2), RNA-seq (n=3), and CUT&RUN (n=2) datasets in HEK293T cells expressing VGLL2-NCOA2 or YAP^{5SA}.
B. Venn diagrams showing the overlaps of ATAC-seq peaks, CUT&RUN peaks, and differentially regulated genes from RNA-seq in HEK293T cells expressing VGLL2-NCOA2 or YAP^{5SA}.
C. KEGG pathway enrichment analysis of ATAC-seq peaks identified in HEK293T cells expressing VGLL2-NCOA2 or YAP^{5SA}. The "Hippo signaling pathway" is highlighted in red.
D. Distribution of CUT&RUN binding sites for VGLL2-NCOA2 and YAP^{5SA}.
E. Motif enrichment analysis of VGLL2-NCOA2 and YAP^{5SA} CUT&RUN Peaks.
F. Genomic tracks showing VGLL2-NCOA2 and YAP^{5SA} occupancy at the CTGF, ANKRD1, and CYR61 loci.

Figure 4. VGLL2-NCOA2 and TEAD1-NCOA2 engage p300 epigenetic regulators.
A. Diagram showing the BioID proteomic analyses of BirA*-VGLL2-NCOA2, BirA*-TEAD1-NCOA2, BirA*-YAP^{5SA}, and BirA*-TAZ^{4SA}.
B. Co-IP assay showing endogenous p300 binding to VGLL2-NCOA2 and TEAD1-NCOA2 but not YAP^{5SA}.
C. KEGG enrichment analysis of p300 CUT&RUN peaks in control HEK293T cells and HEK293T cells expressing VGLL2-NCOA2 or TEAD1-NCOA2. The "Hippo signaling pathway" is highlighted in red.
D. Motif enrichment analysis of p300 CUT&RUN peaks in control HEK293T cells and HEK293T cells expressing VGLL2-NCOA2 or TEAD1-NCOA2.
E. Genomic tracks showing p300 occupancy at the CYR61, ANKRD1, CTGF, and CREB3 loci in control HEK293T cells and HEK293T cells expressing VGLL2-NCOA2 or TEAD1-NCOA2.

Figure 5. p300 is required for VGLL2-NCOA2- and TEAD1-NCOA2-induced tumorigenesis *in vitro*.
A. Co-IP assay showing the NCOA2 fusion part of VGLL2-NCOA2 was essential for p300 binding. VGLL2-NCOA2-V5，VGLL2-$NCOA2^{\triangle NCOA2}$-V5 and VGLL2-$NCOA2^{\triangle VGLL2}$-V5 was expressed in HEK293T cells and immunoprecipitated with an anti-V5 antibody. Endogenous p300 proteins were detected by anti-p300 antibody.

B-D. mRNA levels of Ctgf, Ankrd1, and Cyr61 in C2C12 cells expressing YAP^{5SA}, VGLL2-NCOA2, or TEAD1-NCOA2 with or without treatment of A485 (5 μM). n=3; ****, $p < 0.0001$. NS, no significance.

E. Representative image of colony formation of C2C12 cells expressing YAP^{5SA}, VGLL2-NCOA2, or TEAD1-NCOA2 with or without treatment of A485 (5 μM) for 2 weeks. Scale bars, 100 μm.

F-G. Colony size (F) and number of colonies (G) formed by C2C12 cells expressing YAP^{5SA}, VGLL2-NCOA2, or TEAD1-NCOA2 with or without treatment of A485 (5 μM). **, $p < 0.01$. ****, $p < 0.0001$. NS, no significance.

Figure 6. p300 is essential for VGLL2-NCOA2- and TEAD1-NCOA2-induced tumorigenesis *in vivo*.

A. Representative H&E and IHC staining of Desmin and Ki67 in C2C12-control allograft, C2C12-VGLL2-NCOA2 tumor allograft, and C2C12-TEAD1-NCOA2 tumor allograft. Scale bars, 200 μm.

B. Immunoblot analysis of VGLL2-NCOA2-FLAG and TEAD1-NCOA2-FLAG expression in C2C12 cells, detected by an anti-FLAG antibody.

C-D. Allograft leg volume of C2C12-VGLL2-NCOA2 (C) and C2C12-TEAD1-NCOA2 (D) after intramuscular injection into the leg of Nude mice with or without intraperitoneal injection of A485 (100 mg/kg). The error bars represent the mean leg volume $\pm$ SEM. n = 6. ****, $p < 0.0001$.

E. Representative H&E and IHC staining of Ki67 in C2C12-VGLL2-NCOA2 and C2C12-TEAD1-NCOA2 tumor allografts with or without A485 (100 mg/kg) treatment. Scale bars, 200 μm.

F. Percentage of Ki67-positive cells in Figure 6E. n=6; ***, $p < 0.001$.

G-H. mRNA levels of Ctgf, Ankrd1, and Cyr61 in C2C12-VGLL2-NCOA2 and C2C12-TEAD1-NCOA2 tumor allografts with or without A485 (100 mg/kg) treatment. **, $p < 0.01$. ***, $p < 0.001$. ****, $p < 0.0001$.

Supplement figure legends

Figure 1-figure supplement 1: VGLL2-NCOA2 regulates TEAD-dependent reporter activity.

A. Schematic representation of the exons and breaking points of the VGLL2, TEAD1 and NCOA2 genes involved in generating VGLL2::NCOA2 and TEAD1::NCOA2 gene arrangement.

B. EdU staining showing cell proliferation of HEK293T cells transfected with VGLL2-NCOA2 or TEAD1-NCOA2. Bar chart showing the percentage of EdU-positive cells. Scale bars, 200 μm, n=3; **, $p < 0.01$.

C. Immunoblot analysis of VGLL2-NCOA2, VGLL2-NCOA2$^{\Delta VGLL2}$ and VGLL2-NCOA2$^{\Delta NCOA2}$ in HEK293T cells transfected with the expression constructs carrying the V5 tag.

D. TBS-Luc reporter activity in HEK293T cells expressing VGLL2-NCOA2, VGLL2-NCOA2$^{\Delta VGLL2}$, and VGLL2-NCOA2$^{\Delta NCOA2}$. n = 3. ****, $p < 0.0001$.

E. Immunoblot analysis of VGLL2-NCOA2-V5 in HEK293T cells transfected with different amount of expression constructs.

F. VGLL2-NCOA2 promotes the activation of TBS-Luc reporter in dose-dependent manner. n = 3. ***, $p < 0.001$; ****, $p < 0.0001$.

G-H. Relative mRNA levels of CTGF, ANKRD1, and CYR61 in HEK293T cells expressing VGLL2-NCOA2 (G) or TEAD1-NCOA2 (H) with HA (5' end), FLAG (3' end) or V5 (3' end) tag. n=3; NS, no significance.

Figure 3-figure supplement 1: Analysis of VGLL2-NCOA2, TEAD1-NCOA2 and YAP^{5SA} -induced transcriptomes.

A. Volcano maps of RNA-seq data sets of HEK293T cells expressing VGLL2-NCOA2, TEAD1-NCOA2, or YAP^{5SA}. Red dots represent upregulated mRNAs. Blue dots represent downregulated mRNAs. $p < 0.05$, Log_2FoldChange > 1 or < -1.

B. Veen diagram showing the overlaps of differentially regulated genes identified by RNA-seq in HEK293T cells expressing VGLL2-NCOA2, TEAD1-NCOA2, or YAP^{5SA}.

C. KEGG pathway enrichment analysis of differentially regulated genes identified by RNA-seq in HEK293T cells expressing VGLL2-NCOA2, TEAD1-NCOA2 or YAP^{5SA}. "Hippo signaling pathway" is highlighted in red.

Figure 3-figure supplement 2: ATAC-seq and CUT&RUN data characterization in VGLL2-NCOA2 and YAP^{5SA}-expressing cells.

A. Heatmaps of TEAD-motif containing ATAC-seq peaks in HEK293T cells expressing VGLL2-NCOA2 or YAP^{5SA}.

B. Distribution of ATAC-seq peaks in HEK293T cells expressing VGLL2-NCOA2 or YAP^{5SA}.

For VGLL2-NCOA2 ATAC-seq peaks, Promoter (<=1kb) 50.57%, Promoter (1−2kb) 6.59%, 5' UTR 0.13%, 3' UTR 1.44%, Exon 1.52%, Intron 18.39%, and Distal and Intergenic 21.35%.

For YAP^{5SA} ATAC-seq peaks, Promoter (<=1kb) 51.4%, Promoter (1−2kb) 6.89%, 5' UTR 0.13%, 3' UTR 1.45%, Exon 1.58%, Intron 17.28%, and Distal and Intergenic 21.26%. n=2.

C. VGLL2-NCOA2 promotes chromatin accessibility. Scatter diagrams of ATAC-seq peaks show more up-regulated (red) than downregulated (blue) in HEK293T cells transfected with VGLL2-NCOA2 or YAP^{5SA}.

D. Heatmaps of VGLL2-NCOA2 and YAP^{5SA} CUT&RUN peaks.

E. VGLL2-NCOA2 and YAP genomic occupancy. Scatter diagrams showing more up-regulated CUT&RUN peaks (red) than down-regulated CUT&RUN peaks (blue) of VGLL2-NCOA2 and YAP^{5SA}.

F. KEGG pathway enrichment analysis of VGLL2-NCOA2 and YAP^{5SA} CUT&RUN peaks. “Hippo signaling pathway” is highlighted in red.

Supplementary file legends

Supplementary File 1. RNA-seq analysis showing the genes whose expression was significantly changed in HEK293T cells expressing VGLL2-NCOA2, p-value < 0.05, Log2 Fold Change > 1 or Log2 Fold Change < -1.

Supplementary File 2. RNA-seq analysis showing the genes whose expression was significantly changed in HEK293T cells expressing TEAD1-NCOA2, p-value < 0.05, Log2 Fold Change > 1 or Log2 Fold Change < -1.

Supplementary File 3. RNA-seq analysis showing the genes whose expression was significantly changed in HEK293T cells expressing YAP5SA, p-value < 0.05, Log2 Fold Change > 1 or Log2 Fold Change < -1.

Supplementary File 4. List of specific BioID hits obtained with BirA*-YAP^{5SA}, BirA*-TAZ^{4SA}, BirA*-VGLL2-NCOA2, and BirA*-TEAD1-NCOA2.

Source data file legends

Figure 1, Source Data 1. Original western blot membranes corresponding to Figure 1B indicating the relevant bands. The molecular weight markers are indicated.

Figure 2, Source Data 1. Original western blot membranes corresponding to Figure 2A, 2B, 2C, 2F and 2G indicating the relevant bands. The molecular weight markers are indicated.

Figure 4, Source Data 1. Original western blot membranes corresponding to Figure 4B indicating the relevant bands. The molecular weight markers are indicated.

Figure 5, Source Data 1. Original western blot membranes corresponding to Figure 5A indicating the relevant bands. The molecular weight markers are indicated.

Figure 6, Source Data 1. Original western blot membranes corresponding to Figure 6B indicating the relevant bands. The molecular weight markers are indicated.

Figure 1-figure supplement 1, Source Data 1. Original western blot membranes corresponding to Figure 1-figure supplement 1C and 1E indicating the relevant bands. The molecular weight markers are indicated

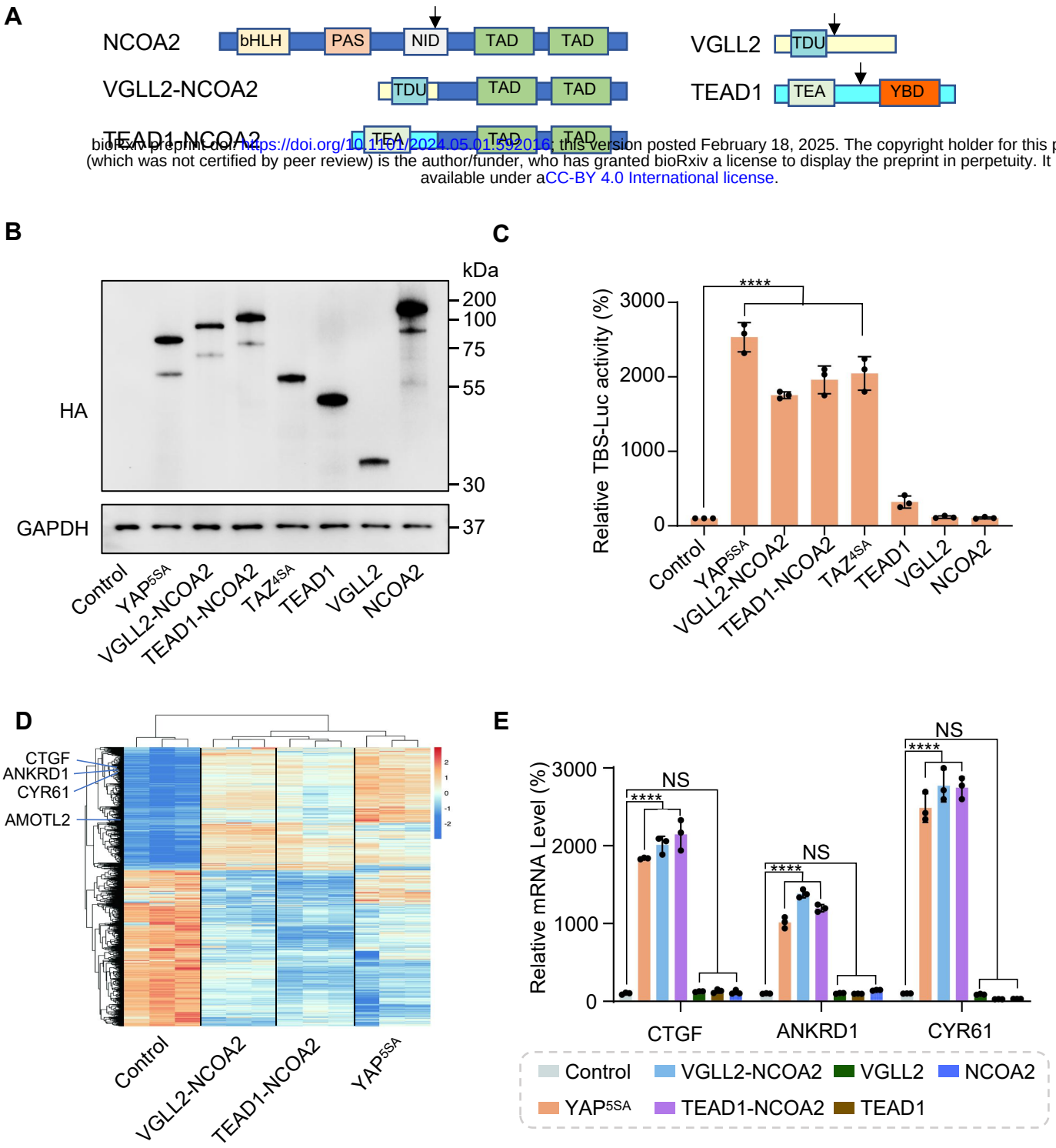

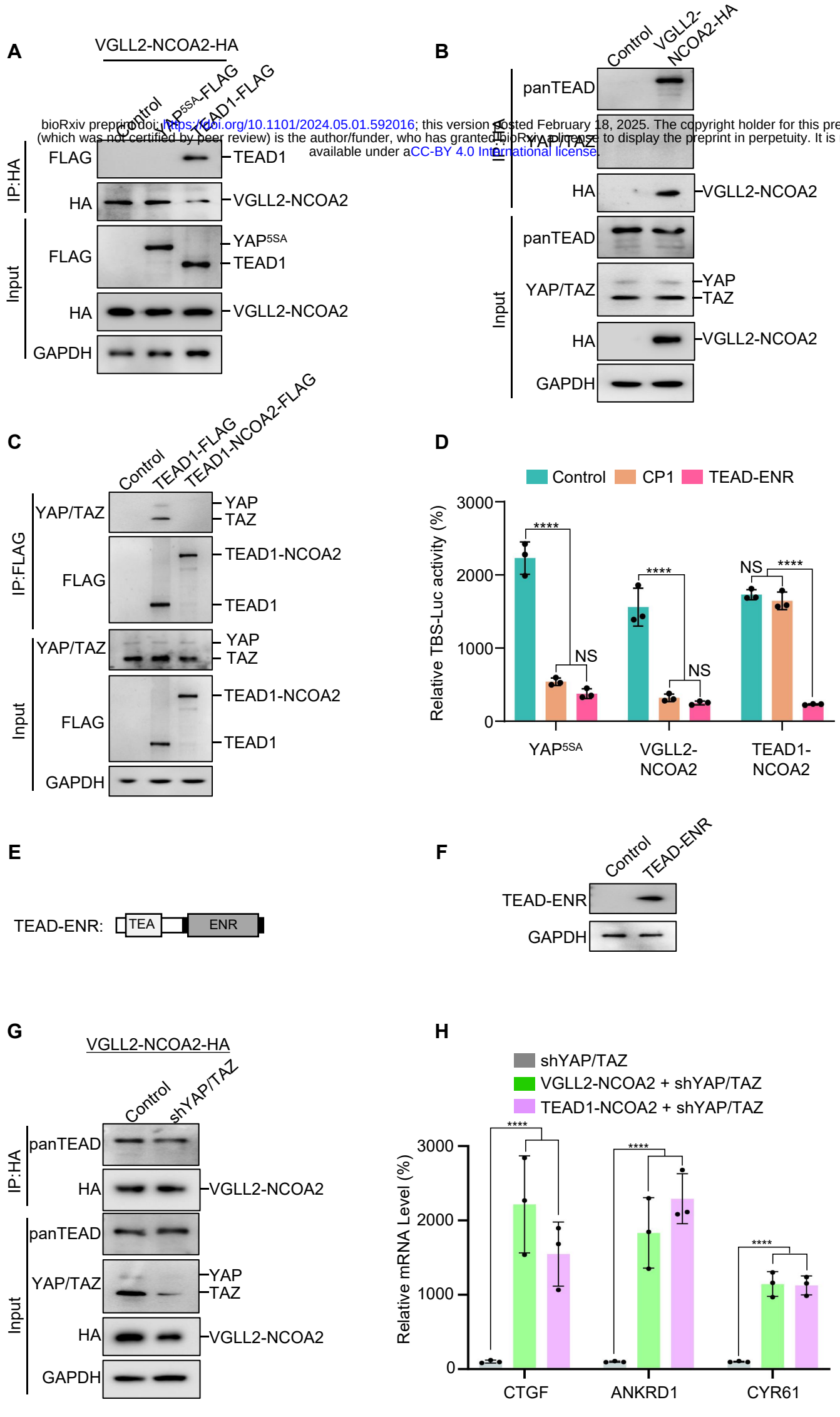

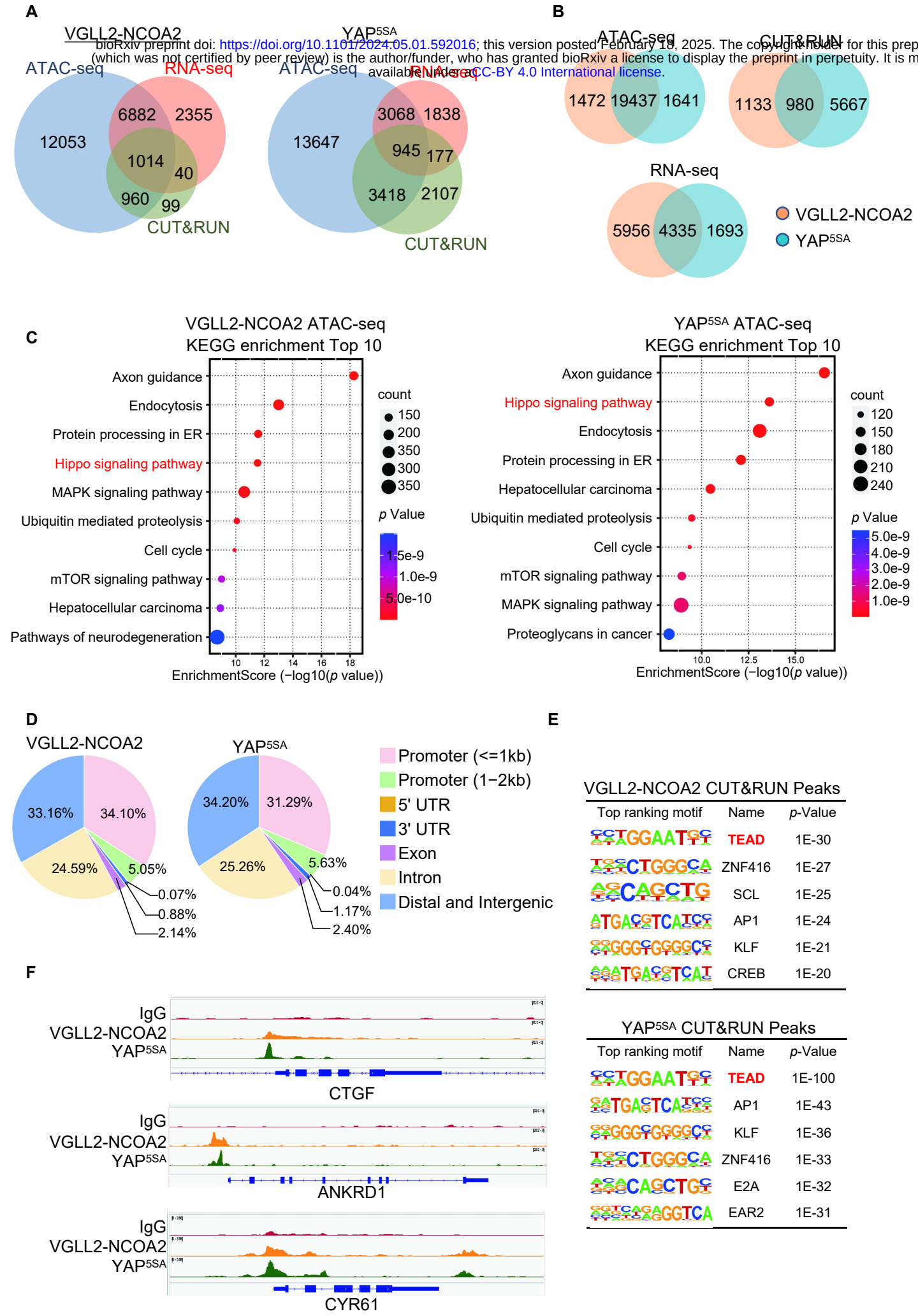

Figure 3. Characterization of VGLL2-NCOA2- and YAP- controlled transcriptional and chromatin landscapes.

A

BioID Proteomic Screens

(BirA*-VGLL2-NCOA2; BirA*-TEAD1-NCOA2; BirA*-YAP^{5SA}; BirA*-TAZ^{4SA})

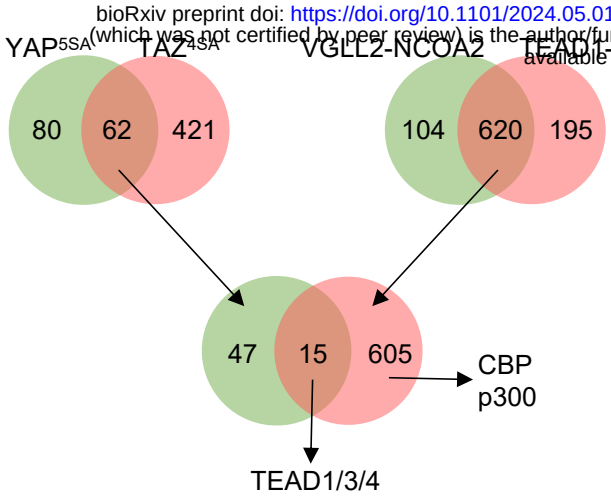

B

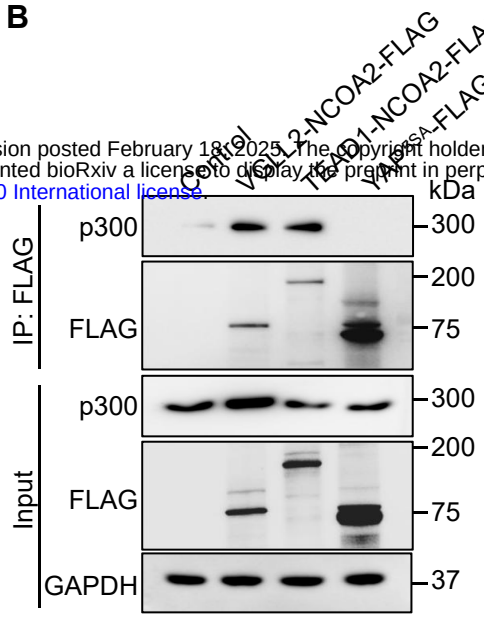

C KEGG term enrichment analysis of p300 CUT&RUN peaks

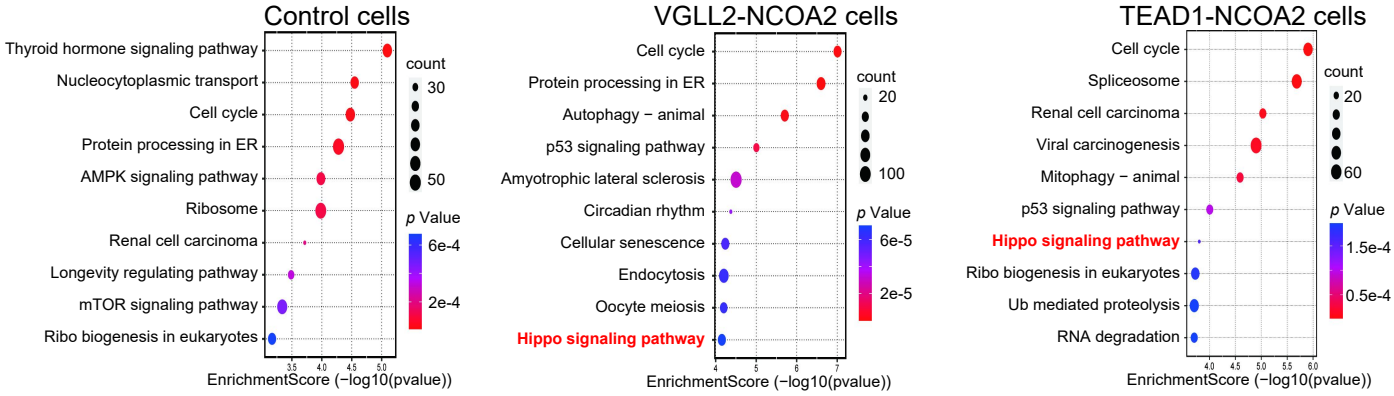

D Motif enrichment analysis of p300 CUT&RUN Peaks

Control cells

Top ranking motif	Name	*p*-value
	NRF	1E-82
	KLF	1E-79
	STAT	1E-40
	Ronin	1E-29
	CREB	1E-19
	ZML2	1E-16

VGLL2-NCOA2 cells

Top ranking motif	Name	*p*-value
	KLF	1E-195
	NRF	1E-97
	AP-1	1E-56
	TEAD	1E-56
	Ronin	1E-50
	CREB	1E-43

TEAD1-NCOA2 cells

Top ranking motif	Name	p-value
	KLF	1E-193
	NRF	1E-99
	Ronin	1E-56
	TEAD	1E-51
	AP-1	1E-46
	CREB	1E-39

E p300 genomic occupancy in control or fusion-expressing cells